A High-resolution Study of the Structure and Conformational Stability of *Pyrococcus horikoshii* Acylphosphatase in Ionic Liquid 1-Ethyl-3-methylimidazolium Tetrafluoroborate by NMR Spectroscopy

LEE, Tsz Ying

A Thesis Submitted in Partial Fulfilment

of the Requirements for the Degree of

Master of Philosophy

in

Biochemistry

The Chinese University of Hong Kong

May 2013

Thesis / Assessment Committee

Professor W.P. Fong (Chair)

Professor K.B. Wong (Thesis Supervisor)

Professor T.F. Chan (Committee Member)

Professor Y.K. Cheng (External Examiner)

Abstract

The extensive application of ionic liquid in biocatalysis and protein chemistry in the past decade arouses interest in the characterization of protein behavior in ionic liquid. This study demonstrates the use of multi-dimensional nuclear magnetic resonance (NMR) spectroscopy to investigate the structure and conformational stability of protein in ionic liquid at a high resolution for the first time, with *Pyrococcus horikoshii* acylphosphatase (PhAcP) and 50% (v/v) 1-ethyl-3-methylimidazolium tetrafluoroborate ([EMIM][BF_4]) as a study model. The backbone amide resonances of PhAcP in 50% (v/v) [EMIM][BF_4] were assigned in order to obtain the chemical shifts of $^{13}C^{\alpha}$, $^{13}C^{\beta}$, ^{13}CO, ^{15}N, H^N and H^{α} of each assigned residue. The estimation of secondary structure by the ^{13}C secondary shift analysis and the nuclear Overhauser effect (NOE) connectivities observed within secondary structures together suggest that PhAcP has secondary structures arranged in native-like topology and there is no major alteration in the tertiary structure in 50% (v/v) [EMIM][BF_4]. Guanidine thiocyanate (GdnSCN)-induced denaturation was performed at 318K, 328K and 338K and monitored by 2D ^{1}H-^{15}N HSQC experiments to study the conformational stability of PhAcP in 50% (v/v) [EMIM][BF_4]. The overlapping denaturation curves and consistent $[GdnSCN]_{1/2}$ values obtained at each temperature indicate no observable trend of stability alteration.

摘要

近十年間，離子液體在生物催化和蛋白質化學方面的廣泛應用引起了鑒定蛋白質在離子液體中特性的研究興趣。本研究以古菌 *Pyrococcus horikoshii* 的酰基磷酸酶 acylphosphatase (PhAcP) 和 50% (v/v) 離子液體 1-乙基-3-甲基咪唑四氟硼酸鹽 ([EMIM][BF_4]) 作為研究模型，首次利用多維核磁共振譜對蛋白質在離子液體中的結構和穩定性作高解析度的分析。我們首先通過蛋白質主鏈共振歸屬，得出 PhAcP 每個被歸屬的胺基酸在 50% (v/v) [EMIM][BF_4] 中 $^{13}C^{\alpha}$、$^{13}C^{\beta}$、^{13}CO、^{15}N、H^N 和 H^{α} 原子的化學位移。^{13}C 的化學位移相對無序纏捲狀態的 ^{13}C 化學位移的偏差分析 (^{13}C secondary shift)，以及二級結構之間的 nuclear Overhauser effect (NOE) 連接顯示 PhAcP 在 50% (v/v) [EMIM][BF_4] 中的二級結構與 PhAcP 的自然結構大致相同，其三級結構亦無顯著變化。此外，我們以二維的 ^{1}H-^{15}N HSQC 實驗觀察在 318K、328K 和 338K 這三個溫度下的硫氰酸胍 (GdnSCN) 誘導蛋白質變性，發現同一溫度下無論 50% (v/v) [EMIM][BF_4]是否存在，PhAcP 的變性曲線都互相重疊，得到的 $[GdnSCN]_{1/2}$ 值也相同，由此可推斷 50% (v/v) [EMIM][BF_4] 對 PhAcP 的穩定性沒有影響。

Acknowledgements

My utmost gratitude goes to my supervisor, Dr. Kam-Bo Wong, for his unlimited guidance, support, patience and timely encouragement. His insight and enthusiasm give me inspiration and motivation. I learn from him the way to be a scientist and more importantly to be a better person. I am indebted to him.

I would like to thank Dr. Ka-Ming Lee, Dr. Tsz-Ha Yu and Dr. Eric Chi-Ho Chan for their generous support for this project. In particular, without all the help from Dr. Ka-Ming Lee concerning NMR spectroscopy, I would not have come so far. Special thanks are addressed to Dr. Ivan Yu-Hang Fong for his sarcastic yet adorable words, and Ms. Fang Luo for the in-depth friendship we share. I am so blessed to have everyone in my group around me.

My deepest appreciation is reserved for my family and my fiancé Mr. Yu-Tong Tam. The effort they made to back me up for anything I want to achieve is so much valuable and incomparable. They are the center of my universe.

This MPhil study is an unexpected journey, regarding both the challenge and the many fruits it brings. I thank God for leading me through.

Contents

Abbreviations

1D	One-dimensional
2D	Two-dimensional
3D	Three-dimensional
CALB	*Candida antarctica* lipase B
DSC	Differential scanning calorimetry
DSS	4,4-Dimethyl-4-silapentane-1-sulfonic acid
[EMIM][BF_4]	1-Ethyl-3-methylimidazolium tetrafluoroborate
FTIR	Fourier transform infrared spectroscopy
GdnSCN	Guanidine thiocyanate
$[GdnSCN]_{1/2}$	Concentration of guanidine thiocyanate at which half the amount of protein is denatured
HSQC	Heteronuclear single quantum coherence
IPTG	Isopropyl-β-D-thiogalactopyranoside
LB	Luria-Bertani
NMR	Nuclear magnetic resonance
NOE	Nuclear Overhauser effect
NOESY	Nuclear Overhauser effect spectroscopy
PAGE	Polyacrylamide gel electrophoresis
PhAcP	*Pyrococcus horikoshii* acylphosphatase
SDS	Sodium dodecyl sulphate
TOCSY	Total correlation spectroscopy
Tris	Tris(hydroxymethyl)aminomethane

Amino Acids

Ala	A	Alanine	Leu	L	Leucine
Arg	R	Arginine	Lys	K	Lysine
Asn	N	Asparagine	Met	M	Methionine
Asp	D	Aspartate	Phe	F	Phenylalanine
Cys	C	Cysteine	Pro	P	Proline
Gln	Q	Glutamine	Ser	S	Serine
Glu	E	Glutamate	Thr	T	Threonine
Gly	G	Glycine	Trp	W	Tryptophan
His	H	Histidine	Tyr	Y	Tyrosine
Ile	I	Isoleucine	Val	V	Valine

List of Figures

List of Tables

Chapter 1 Introduction

1.1 Introduction to ionic liquid

1.1.1 Ionic liquid as reaction medium, co-solvent and additive in biocatalysis and protein chemistry

Ionic liquid is basically molten salt. The typical classes of ionic liquids consist of an organic cation (e.g. alkylammonium, dialkylimidazolium, alkylpyridinium, and dialkylpyrrolidinium) and an inorganic or organic anion (e.g. chloride, tetrafluoroborate, and hexafluorophosphate, and trifluoromethylsulfonate). The bulkiness of both ions contributes to the low melting temperature of ionic liquid.

In the past decade, the application of ionic liquid in various industrial and research processes was receiving increasing attention. In particular, the replacement of organic solvent by ionic liquid in enzyme-catalyzed organic synthesis was extensively explored since 2000 (Erbeldinger et al., 2000; Van Rantwijk & Sheldon, 2007). Organic synthesis involving non-polar substrates and water as a by-product is conventionally performed in organic solvents to improve reaction rate and yield. Yet the use of organic solvents leads to practical and environmental concerns due to their

volatile, toxic and flammable nature. Ionic liquid is a potential alternative with negligible vapor pressure, low flammability and high thermal stability. On top of that, it is also a "designer solvent" of which the physicochemical properties including polarity, density, viscosity, melting point, kosmotropicity, and miscibility with water or organic solvents can be engineered with a wide range of ion combinations for specific biocatalytic reactions.

Aside from being a reaction medium, ionic liquid is also found useful as a co-solvent and an additive in various applications with protein. Fujita and coworkers (2005) reported the use of N-butyl-N-methylpyrrolidinium dicyanamide with 20% (w/w) water to increase the solubility of cytochrome c. Summers and Flowers (2000) demonstrated the ability of 5% (v/v) ethylammonium nitrate to enhance the renaturation of denatured hen egg white lysozyme by preventing aggregation in the refolding process. Later, similar refolding enhancement of hen egg white lysozyme and a single-chain antibody fragment ScFvOx was also observed in a series of N'-alkyl and N'-(ω-hydroxy-alkyl)-N-methylimidazolium chlorides (Lange et al., 2005). Recently, there is a growing interest in using ionic liquid as additive in protein crystallization since the illustration of its potential to improve protein crystallization behavior and the diffraction quality of protein crystals (Hekmat et al., 2007; Judge et

al., 2009). The wide-ranged and finely tunable polarity of ionic liquid also makes it useful in liquid chromatography and capillary electrophoresis for protein purification and analysis (Marszałł & Kaliszan, 2007).

1.1.2 The impact of ionic liquid on protein structure and stability is poorly understood

Regarding the extensive application of ionic liquid with protein, it is essential to address the biocompatibility of ionic liquid. Previous studies of the properties of protein in ionic liquid focus on the characterizations of solubility, structure, stability, activity and selectivity (Naushad et al., 2012). Yet there is still no conclusive correlation between the ion properties and the behavior of protein. The observed impact of each ionic liquid species seems concentration-specific, protein-specific and reaction-specific.

The description of protein structure in ionic liquid in literature is generally in terms of tertiary structure, secondary structure and hydrodynamic radius in comparison with that of the native protein in buffer. Nevertheless, none of the assays involved can provide a detailed and unambiguous picture of the protein structure.

They can only probe for change in protein structure as compared to the native one, but cannot indicate what the change is. For instance, protein tertiary structure is implied by its enzymatic activity (Bihari et al., 2010; Weaver et al., 2012) or the intrinsic fluorescence (De Diego et al., 2005). Recently a dye that emits fluorescence upon binding to the hydrophobic patch of protein is also employed to monitor protein unfolding (Rodrigues et al., 2011). Yet enzymatic activity is not a representation solely of protein tertiary conformation, but a complex function of protein and substrate solubility, protein conformation and reaction yield. The approach involving fluorescence is complicated by the impact of ionic liquid on fluorescence (Bekhouche et al., 2012). There is additional concern for the solubility of the fluorescent dye in ionic liquid. The strategies to measure secondary structures include circular dichroism (Bihari et al., 2010; De Diego et al., 2004, 2005; Sasmal et al., 2011; Sen Mojumdar et al., 2012) and fourier transform infrared spectroscopy (FTIR) (Bihari et al., 2010; Fujita et al., 2005; Lau et al., 2004). Both of the assays make use of the spectral region which is strongly interfered by common ionic liquids. The hydrodynamic radius is determined by viscosity (Bihari et al., 2010; Sasmal et al., 2011; Sen Mojumdar et al., 2012) which is largely increased in the presence of ionic liquid.

Effort is put in establishing the Hofmeister series of ionic liquid, in which common ions of ionic liquid are arranged in the order of their influence on the stability of protein conformation (Constantinescu et al., 2007; Zhao et al., 2006a, 2006b). In these studies, the stability of protein in ionic liquid is often indicated by its melting temperature determined in thermal denaturation. The loss of protein conformation upon thermal denaturation is detected by protein intrinsic fluorescence (Baker et al., 2004; De Diego et al., 2004; Heller et al., 2010), residual activity of enzymes (De Diego et al., 2004, 2005; De Los Ríos et al., 2007; Ebrahimi et al., 2012; Ha et al., 2008; Noritomi et al., 2011), circular dichroism (Huang et al., 2011; Weaver et al., 2012) and differential scanning calorimetry (DSC) (Constantinescu et al., 2007; De Diego et al., 2004; Fujita et al., 2005). Based on the shortcoming of the aforementioned assays, DSC serves as a better probe for conformational change upon denaturation. However, uninterpretable DSC profile is still occasionally obtained for protein in ionic liquid (De Diego et al., 2004; Fujita et al., 2005). This may be attributed to the fact that DSC measures any heat changes in the denaturation process instead of specifically monitoring the protein conformation after all.

The lack of unambiguous assaying methods in previous studies poses difficulty on the discussion of the effect of ionic liquid on protein structure and stability.

Therefore, in this study, multi-dimensional nuclear magnetic resonance (NMR) spectroscopy is employed in an attempt to acquire a more comprehensive understanding to the structure and hence the conformational stability of protein in ionic liquid. The selection of model protein and ionic liquid is discussed in the following section.

1.2 PhAcP in [EMIM][BF_4] as a model to study the structure and stability of protein in ionic liquid by NMR spectroscopy

1.2.1 The application of [EMIM][BF_4] with protein

1-Ethyl-3-methylimidazolium tetrafluoroborate ([EMIM][BF_4]; Figure 1.1) is a representative member of the dialkylimidazolium-based ionic liquid, which is one of the most commonly investigated classes of ionic liquid in both industry and academia. Due to the similar polarity of [EMIM][BF_4] to conventional hydrophilic organic solvents used in industrial biocatalysis (Carmichael & Seddon, 2000), the possibility of replacing organic solvents by [EMIM][BF_4] is immensely explored. In particular, [EMIM][BF_4] is mainly employed as a reaction medium in lipase-catalyzed synthetic biotransformations. Examples include the *Candida antarctica* lipase B (CALB)-catalyzed amide synthesis (Irimescu & Kato, 2004) and

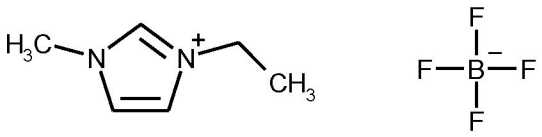

Figure 1.1. The chemical structure of [EMIM][BF_4].

synthesis of butyl butyrate by transesterification (Lozano et al., 2001a, 2003) performed in ≥ 98% (v/v) [EMIM][BF_4]. The activity and half-life of CALB were found increased in the synthetic reactions of butyl butyrate and specific amides. The biocompatibility of [EMIM][BF_4] in transesterification was also demonstrated by the α-chymotrypsin-mediated N-acetyl-L-tyrosine propyl ester synthesis (Lozano et al., 2001b, 2003) as well as the polymerization of ε-caprolactone by *Yarrowia lipolytica* lipase (Barrera-Rivera et al., 2009). In 2010, the use of [EMIM][BF_4] even expanded to whole-cell biocatalysis for biodiesel fuel production (Arai et al., 2010). The biodiesel fuel is a fatty acid methyl ester produced from the transesterification of triglyceride and methanol catalyzed by lipase-producing fungi in ≤ 50% (v/v) [EMIM][BF_4]. [EMIM][BF_4] can possibly serve as a reservoir for the substrate methanol and the by-product glycerol. As a result, the fungal lipase is found no longer deactivated by a high concentration of methanol like it is in the conventional system. The extraction of glycerol can also reduce product inhibition.

The involvement of [EMIM][BF_4] in protein science is emerging more recently. Judge and coworkers (2009) reported the use of 3-36% (v/v) [EMIM][BF_4] as an additive in protein crystallization to enhance crystallization behavior (i.e. increase in crystal size, change in morphology) and X-ray diffraction quality. [EMIM][BF_4] is

also applied in liquid chromatography and capillary electrophoresis to improve the resolution in protein purification and analytical chemistry (Marszałł & Kaliszan, 2007).

1.2.2 The background of PhAcP

Pyrococcus horikoshii acylphosphatase (PhAcP) is a hyperthermophilic archaeal acylphosphatase (E.C. 3.6.1.7) with an apparent melting temperature of 111.5°C (384.5K) (Cheung et al., 2005). It catalyzes the hydrolysis of the carboxyl-phosphate bond and is involved in various physiological processes including glycolysis, tricarboxylic acid cycle and pyrimidine and urea biosynthesis (Stefani et al., 1997). In 2005, our group has solved the crystal structure of PhAcP (PDB code 1W2I) and characterized its thermostability and catalytic activity (Cheung et al., 2005). The crystal structure of this small enzyme (91 amino acid residues) reveals an α/β sandwich fold consisting of two helices packed on a five-stranded β-sheet. The extensive ion-pair network on the surface of the β-sheet is suggested to contribute to the extreme thermostability of PhAcP.

Considered the excellent ability of PhAcP to resist denaturation and the

previous experience of our group to characterize this enzyme, PhAcP is selected as the model protein to start with the study of the influence of ionic liquid ([EMIM][BF_4] as a model) on protein structure and stability.

1.2.3 Overview of the study

This study is concerned with the structure and stability characterization of PhAcP in ionic liquid [EMIM][BF_4] by means of multi-dimensional NMR spectroscopy. NMR is a powerful tool that provides an atomic-level investigation of PhAcP. Therefore, unlike conventional assays, it enables a direct and unambiguous address to the conformation of protein. The strategy of triple resonance experiments in NMR spectroscopy also confers superiority to the conventional assays of protein characterization including the spectroscopic detection at 280 nm and circular dichroism, which are overwhelmingly interfered by the strong absorption of [EMIM][BF_4] in the far-UV spectral region.

The study began with the determination of the suitable [EMIM][BF_4] concentration for the characterization of PhAcP by NMR spectroscopy. After that, backbone resonance assignment of PhAcP in [EMIM][BF_4] was performed as a

crucial step to the analysis of further NMR experiments. The backbone assignment allows the chemical shifts of $^{13}C^{\alpha}$, $^{13}C^{\beta}$, ^{13}CO, ^{15}N, H^{N} and H^{α}, which indicate the chemical environment of the concerned atom, to be obtained for each amino acid residue.

With the knowledge of $^{13}C^{\alpha}$ and $^{13}C^{\beta}$ chemical shifts from the backbone assignment, the structure of PhAcP in [EMIM][BF_4] was determined by the ^{13}C secondary shift, which is an estimation of the protein secondary structure (Spera & Bax, 1991; Wishart et al., 1991). On the other hand, the phenomenon of nuclear Overhauser effect (NOE), which detects protons in close proximity, within α-helix and β-sheet also provided independent structural information (Kumar et al., 1980).

The conformational stability of PhAcP in [EMIM][BF_4] was determined by guanidine thiocyanate-induced denaturation probed by 2D ^{1}H-^{15}N HSQC experiments (Bodenhausen & Ruben, 1980). Denaturation curves and $[GdnSCN]_{1/2}$ values were obtained for stability characterization.

Chapter 2 Materials and Methods

2.1 Expression and purification of PhAcP

2.1.1 Expression of PhAcP in Escherichia coli system

The clone of PhAcP in pET8c vector is a gift from Dr. Tsz-Ha Yu. A volume of 0.5 μl plasmid was added to 100 μl *Escherichia coli* C41(DE3) competent cells and incubated on ice for 5 minutes. The tube was then transferred to heat block at 42°C for 2-minute incubation and then placed back on ice for 5 minutes. The cells were evenly plated onto a Luria-Bertani (LB) agar plate [1] containing 100 μg/ml ampicillin for selection. The plate was incubated upside down at 37 °C for 16-20 hours.

---

[1] **LB agar:** 1% (w/v) bacto-tryptone, 0.5% (w/v) yeast extract, 1% (w/v) NaCl, 1.5% (w/v) bacto-agar

A single colony obtained on the plate was picked and inoculated into 10 ml culture medium (LB [2] for unlabelled protein and minimal medium [3] for labelled protein) containing 100 μg/ml ampicillin. This starter culture was incubated at 37°C with continuous shaking at 250 rpm for 16-20 hours.

After incubation, the culture was inoculated (1% v/v) into 1 L of fresh culture medium containing 100 μg/ml ampicillin. The 1 L culture was then separated equally into two 2 L flask to allow enough aeration for bacterial growth. The expression culture was incubated at 37°C with continuous shaking at 250 rpm until its absorbance at 600 nm reached 0.4-0.8. The expression of PhAcP was induced by

---

[2] **LB:** 1% (w/v) bacto-tryptone, 0.5% (w/v) yeast extract, 1% (w/v) NaCl

[3] **M9:** 0.6% (w/v) $Na_2HPO_4 \cdot 7H_2O$, 0.3% (w/v) KH_2PO_4 (anhydrous), 0.05% (w/v) NaCl, 1 mM $MgSO_4$, 0.4% (v/v) Solution Q [4], freshly prepared Vitamin Mix [5], 0.4% (w/v) glucose or ^{13}C-labelled glucose, 0.1% (w/v) NH_4Cl or ^{15}N-labelled NH_4Cl

[4] **Solution Q:** 0.8% (v/v) 5N HCl, 0.5% (w/v) $FeCl_2 \cdot 4H_2O$, 0.0184% (w/v) $CaCl_2 \cdot 2H_2O$, 0.0064% (w/v) H_3BO_3, 0.0018% (w/v) $CoCl_2 \cdot 6H_2O$, 0.0004% (w/v) $CuCl_2 \cdot H_2O$, 0.034% (w/v) $ZnCl_2$, 0.0605% (w/v) $Na_2MoO_4 \cdot 2H_2O$, 0.004% (w/v) $MnCl_2 \cdot 4H_2O$

[5] **Vitamin Mix:** 0.001% (w/v) Thiamine, 0.0002% (w/v) D-Biotin, 0.0002% (w/v) Choline chloride, 0.0002% (w/v) Folic acid, 0.0002% (w/v) Niacinamide, 0.0002% (w/v) D-Pantothenic acid, 0.0002% (w/v) Pyridoxal, 0.0002% (w/v) Riboflavin

adding 0.4 mM isopropyl-β-D-thiogalactopyranoside (IPTG). At the same time, the medium was also supplemented with 100 μg/ml ampicillin. The expression culture was allowed to grown overnight at 37°C with continuous shaking at 250 rpm. The cells were harvested by centrifugation at 6000×g at 4 °C for 10 min.

2.1.2 Purification of PhAcP

The cell pellet harvested from each litre of culture was resuspended in 20-30 ml of 20 mM Tris-HCl, pH 7.5. The cells were lysed by sonication (Vibra-Cell, Sonic & Materials) on ice at 20-second pulse until the lysate became clear. The lysate was then centrifuged at 12300×g for 1 hour at 4°C. The supernatant which contained PhAcP was filtered through a 0.22 μm filter to remove any cell debris.

PhAcP was purified with column chromatography handled with the ÄKTA prime system (GE Healthcare). The filtered supernatant was loaded into a prepacked 5 ml HiTrap SP HP column (GE Healthcare) pre-washed with 20 mM Tris-HCl, 1 M NaCl, pH 7.5 and pre-equilibrated with 20 mM Tris-HCl, pH 7.5 (Buffer A). After extensive washing with Buffer A, PhAcP was eluted with linear gradient of 0-1 M NaCl over a volume of 150 ml. The elution fractions were analyzed by SDS-PAGE

and those containing semi-purified PhAcP were collected and concentrated to around 5 ml with a centrifugal concentrator (Vivaspin 20, MWCO 3000, GE Healthcare) by ultra-filtration at 4000×g centrifugation.

The concentrated semi-purified protein was filtered through a 0.22 μm filter and loaded into a HiLoad 26/60 Superdex G-75 gel filtration column (GE Healthcare) pre-equilibrated with 20 mM Tris-HCl, 0.2 M NaCl, pH 7.5. Purified PhAcP was dialyzed overnight against 10 mM NaOAc, pH 5.3 and concentrated to 5 mM for further assays.

2.2 Solubility determination

The solubility of PhAcP in various concentrations of [EMIM][BF_4] was determined in a 100 μl mixture of PhAcP, [EMIM][BF_4] (purchased from Tokyo Chemical Industry), and buffer (10 mM NaOAc, pH 5.3). [EMIM][BF_4] of 0, 50, 60, 65, 70, 75, 80, 85 or 90 μl, depending on its final concentration in % v/v in the 100 μl mixture, was first mixed with buffer to reach a volume of 90 μl. Then, 10 μl of 5 mM purified PhAcP was added to the diluted [EMIM][BF_4] to get a final concentration of 0.5 mM. Undissolved precipitated PhAcP was removed by filtration through a

0.2 μm filter (Sartorius). The filter has a chemically highly compatible PTFE membrane with a small diameter of 4 mm to minimize the loss of sample due to membrane hold-on. The [EMIM][BF_4] in the sample was removed by buffer exchange using ultra-filtration: The sample was mixed with 400 μl buffer and subjected to 6800×g centrifugation for 25 minutes in a centrifugal filter (Amicon Ultra-0.5 mL, 3K, Merck Millipore). The ~400 μl flow-through containing [EMIM][BF_4] was discarded. The whole process was repeated 7 times to ensure the amount of [EMIM][BF_4] in the sample was negligible. After that, the sample was recovered from the centrifugal filter as instructed by the manufacturer. The volume was measured and the concentration of PhAcP in the sample was determined by UV-vis spectroscopic measurement at 280 nm (BioPhotometer, Eppendorf). The concentration of soluble PhAcP in M was calculated by:

$$[\text{PhAcP}] = (OD_{280} / \varepsilon) \times (V / V_0) \quad (1)$$

where OD_{280} is the absorbance at 280 nm, ε is the molar extinction coefficient of PhAcP (i.e. 23490 $M^{-1} cm^{-1}$), V is the final volume in μl, and V_0 is the initial volume (i.e. 100 μl). Additional samples with PhAcP replaced by buffer served as the negative control to indicate the sufficient removal of [EMIM][BF_4] by ultra-filtration.

2.3 NMR experiments

2.3.1 General procedures and sample preparation

NMR experiments were acquired with a Bruker Avance III 700 MHz spectrometer. Before each acquisition, deuterium lock (for a stable magnetic field), manual probe tuning and matching (for a higher probe sensitivity) and shimming (for a lower inhomogeneity of the magnetic field) were performed. The offset frequency of the ^{1}H dimension was set to that of the water signal determined in the Bruker 1D water presaturation experiment (ZGPR) in order to achieve water suppression. The ^{1}H 90° pulse width was determined by the Bruker AU program (PULSECAL).

The NMR data were processed with NMRPipe (Delaglio et al., 1995) and analyzed with NMRView (Johnson & Blevins, 1994).

All NMR samples had a volume of 200 µl and were contained in a 3 mm NMR tube (NORELL). Vacuum degassing was performed on the samples before experiments.

2.3.2 ^{1}H-^{15}N HSQC spectra in various concentrations of [EMIM][BF_4]

The ^{1}H-^{15}N HSQC experiments (Bodenhausen & Ruben, 1980) were performed on ^{15}N-labelled PhAcP at 298K. The samples contained 0.5 mM ^{15}N-labelled PhAcP, 10% (v/v), 50% or 70% [EMIM][BF_4] (purchased from Tokyo Chemical Industry), 5 mM 4,4-dimethyl-4-silapentane-1-sulfonic acid (DSS), 5% D_2O and buffer (10 mM NaOAc, pH 5.3) to bring the final volume to 200 μl.

2.3.3 Structural characterization

The sequential assignment of backbone amide resonances was obtained based on the $^{13}C^{\alpha}$, $^{13}C^{\beta}$ and ^{13}CO connectivities observed in the CBCA(CO)NH (Grzesiek & Bax, 1992a), HNCACB (Wittekind & Mueller, 1993), HN(CO)CA (Bax & Ikura, 1991; Grzesiek & Bax, 1992b), HNCA (Farmer et al., 1992; Grzesiek & Bax, 1992b; Kay et al., 1990), HNCO (Grzesiek & Bax, 1992b; Kay et al., 1990; Muhandiram & Kay, 1994) and HN(CA)CO (Clubb et al., 1992) spectra. The long-range inter-proton NOE within secondary structures was determined in the ^{1}H-^{15}N NOESY-HSQC experiment (Bax et al., 1990; Frenkiel et al., 1990) with a mixing time of 120 ms. These triple resonance experiments were acquired on ^{15}N,^{13}C-labelled PhAcP at

298K. The samples contained 0.5 mM ^{15}N,^{13}C-labelled PhAcP, 50% (v/v) [EMIM][BF_4], 5 mM DSS, 5% D_2O and buffer (10 mM NaOAc, pH 5.3) to bring the final volume to 200 µl.

2.3.4 Stability characterization

The conformational stability of PhAcP was determined by guanidine thiocyanate-induced denaturation monitored by ^{1}H-^{15}N HSQC experiments (Bodenhausen & Ruben, 1980), in which ^{15}N-labelled PhAcP in 0% or 50% (v/v) [EMIM][BF_4] was mixed with 0 M – 2 M guanidine thiocyanate in 0.2 M step. Therefore, the NMR samples contained 0.1 mM ^{15}N-labelled PhAcP, 0% or 50% (v/v) [EMIM][BF_4], 0 M – 2 M guanidine thiocyanate, 5 mM DSS, 5% D_2O and buffer (10 mM NaOAc, pH 5.3) to bring the final volume to 200 µl. The ^{1}H-^{15}N HSQC experiments were performed at 318K, 328K and 338K subsequently. The temperature was controlled by the NMR spectrometer. The samples were equilibrated for 5 minutes after each change in temperature.

After data processing, the amide resonances from native PhAcP in the spectra were picked and their intensities were estimated by NMRView (Johnson & Blevins,

1994). The total intensity of all traceable resonances against guanidine thiocyanate concentration was fitted into a two-state model (Santoro & Bolen, 1988) by KaleidaGraph 4.0 (Synergy Software) with the following equation:

$$y = \frac{\left(y_f + m_f[D]\right) + \left(y_u + m_u[D]\right)*\exp\left[-\frac{m\left([\mathrm{GdnSCN}]_{1/2} - [D]\right)}{RT}\right]}{1 + \exp\left[-\frac{m\left([\mathrm{GdnSCN}]_{1/2} - [D]\right)}{RT}\right]} \qquad (2)$$

where y is the y-axis parameter (i.e. total intensity or fraction unfolded), y_f and m_f are the y-intercept and slope of the pre-transition (folded state) baseline, y_u and m_u are the y-intercept and slope of the post-transition (unfolded state) baseline, $[D]$ is the concentration of guanidine thiocyanate, m is the slope of the transition, $[\mathrm{GdnSCN}]_{1/2}$ is the mid-point of transition, R is the gas constant in J K^{-1} mol^{-1}, and T is the temperature in K. In the plot of total intensity against guanidine thiocyanate concentration, m_f, m_u and y_u were set to 0.

With reference to the fitted y_f value (i.e. native resonance intensity at native state), the total intensity was converted into fraction unfolded, which was fitted again into equation (2) with m_f, m_u and y_f set to 0 and y_u set to 1 to obtain the denaturation curve and the $[\mathrm{GdnSCN}]_{1/2}$ value.

Chapter 3 Results

3.1 Can the solubility of PhAcP in [EMIM][BF_4] reach the milli-molar range required for NMR study?

Since NMR experiments require protein concentration in the milli-molar range for an acceptable signal-to-noise ratio, there is a need to determine the solubility of PhAcP as a function of [EMIM][BF_4] concentration first. 5 mM PhAcP was diluted 10-fold in various concentrations of [EMIM][BF_4]. Undissolved precipitated protein was removed by filtration. Due to the strong absorption of [EMIM][BF_4] in the far-UV spectral region, the ionic liquid was removed by buffer exchange using ultra-filtration. The concentration of soluble PhAcP was then determined by UV-vis spectroscopic measurement at 280 nm.

The result illustrated in Figure 3.1 shows that when the concentration of [EMIM][BF_4] is $\leq$ 70% (v/v), the solubility of PhAcP can reach 0.4-0.5 mM which meets the requirement of a feasible NMR study. On the other hand, the [EMIM][BF_4] concentration range $\geq$ 70% (v/v) exhibits a drastic drop in PhAcP solubility, which renders these conditions unsuitable in NMR experiments.

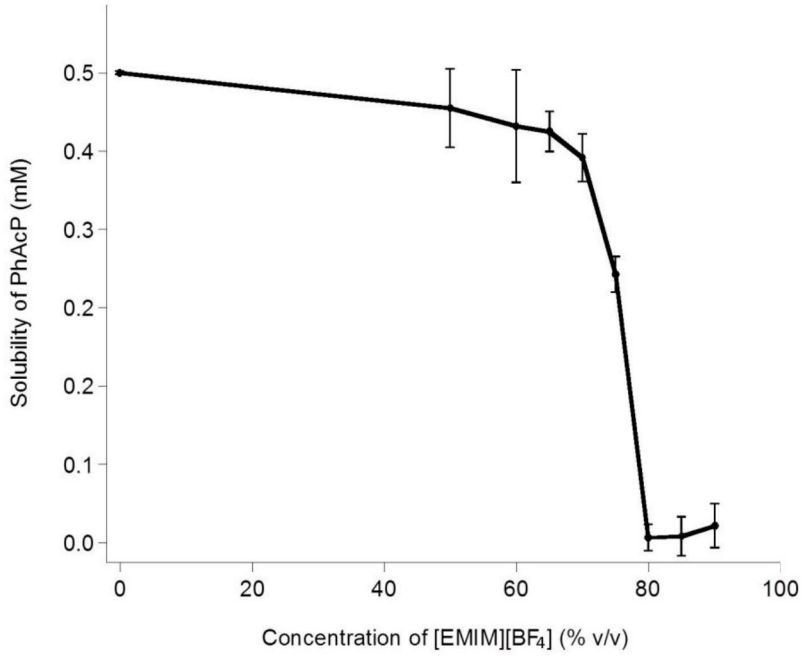

Figure 3.1. The solubility of PhAcP is high enough for NMR studies when the concentration of [EMIM][BF_4] is below 70% (v/v). Protein NMR studies require protein concentration in the milli-molar range. Therefore, 0.5 mM of PhAcP was subjected to [EMIM][BF_4] of various concentrations and its solubility was determined by UV-vis spectroscopic measurement at 280 nm after removal of precipitated protein and ionic liquid. The plot shows the average of three sets and the error bars denote one standard deviation.

3.2 Determination of the [EMIM][BF_4] concentration for a feasible NMR study

Although the solubility of PhAcP in ≤ 70% (v/v) [EMIM][BF_4] is high enough for NMR study, it is necessary to also consider practically the effect of [EMIM][BF_4] on the quality of NMR experiments. The 2D ^{1}H-^{15}N HSQC experiment (Bodenhausen & Ruben, 1980), which correlates backbone ^{1}H and ^{15}N by one-bond coupling, was acquired in the presence of 10% (v/v), 50% and 70% of [EMIM][BF_4] in order to evaluate the interference of [EMIM][BF_4] to the NMR spectrum of PhAcP.

With reference to Figure 3.2, with an increasing concentration of [EMIM][BF_4], the quality of the ^{1}H-^{15}N HSQC spectrum of PhAcP is reduced accordingly. For instance, each isolated dot in the spectrum is the resonance peak of the backbone amide of each amino acid residue in PhAcP. When the concentration of [EMIM][BF_4] is as high as 50% (v/v) and 70%, three streaks of noise appear in the spectrum at 8.95, 7.83 and 7.76 ppm of the ^{1}H dimension in 50% (v/v) [EMIM][BF_4] and at 9.28, 8.17 and 8.07 ppm in 70% (v/v) [EMIM][BF_4]. According to the reported chemical shifts of all protons of [EMIM][BF_4] in its ^{1}H NMR spectrum (Holbrey & Seddon, 1999), the distribution of the three streaks agrees with that of the proton peaks of H^2, H^4 and

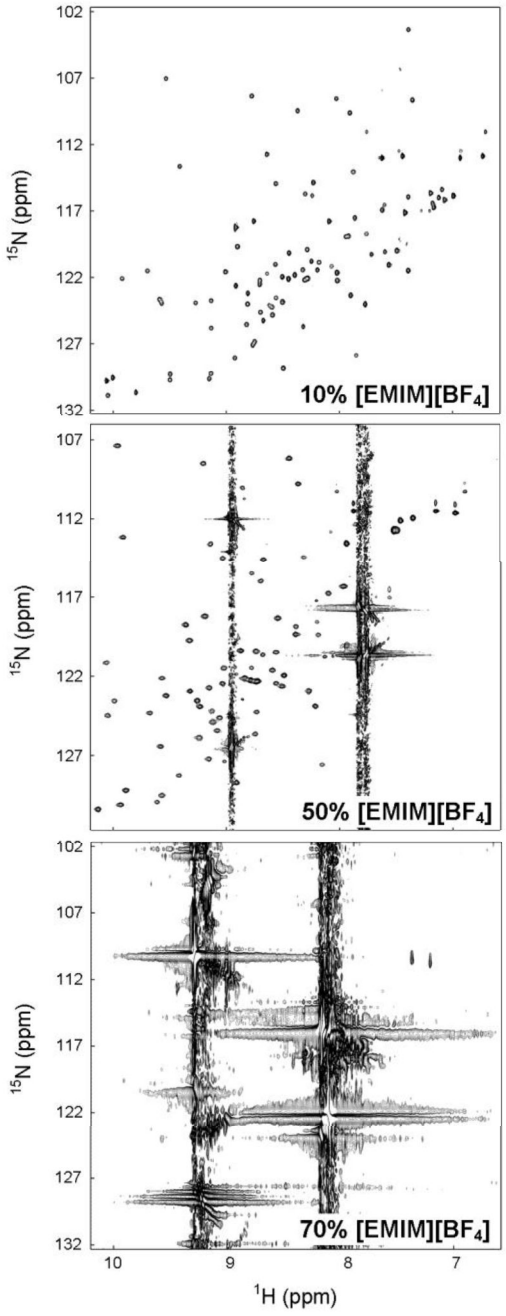

Figure 3.2. In 50% (v/v) [EMIM][BF_4], PhAcP produces a decent ^{1}H-^{15}N HSQC spectrum in a reasonably high concentration of [EMIM][BF_4] at 298K and pH 5.3. Increasing concentration of [EMIM][BF_4] creates overwhelming noise in the ^{1}H-^{15}N HSQC spectrum. The protein signals in the presence of 70% (v/v) [EMIM][BF_4] are immensely masked by the noise. Hence the [EMIM][BF_4] concentration of 50% (v/v) was chosen for further NMR study.

H^5 (8.88, 7.72 and 7.65 ppm) in the imidazolium ring respectively. On top of that, there are specific resonances of N-H coupling observed as distinct intense signals on the streaks. They are attributed to the two-bond coupling of H^2, H^4 and H^5 with N^1 and N^3. Although ^1H-^{15}N HSQC experiment is theoretically specific to the one-bond coupling of ^1H and ^{15}N in labelled molecules, practically the resonance of other N-H coupling can still be detected due to fact that the specificity of the experiment is based on the maximization of the resonance of one-bond coupling but not a complete elimination of the other resonance, and the heavy isotope ^{15}N has a natural abundance of 0.37%. Since [EMIM][BF_4] is in molar concentration while PhAcP is only in milli-molar range, and the relaxation of small molecules like $[EMIM]^+$ is much slower than that of protein macromolecules, the H^2, H^4 and H^5 of $[EMIM]^+$ creates such strong streaks of noise of which the intensity grows with increasing [EMIM][BF_4] concentration.

In 70% (v/v) [EMIM][BF_4], the noise from [EMIM][BF_4] is overwhelming that almost all protein signals are masked, whereas the condition of 50% (v/v) [EMIM][BF_4] produces a decent spectrum in a reasonably high concentration of [EMIM][BF_4]. Therefore, 50% (v/v) was chosen as the [EMIM][BF_4] concentration in the following NMR study.

As a first step to characterize the structure and conformational stability of PhAcP in 50% (v/v) [EMIM][BF_4] by NMR spectroscopy, backbone resonance assignment was performed to acquire information on the chemical environment, in terms of chemical shifts, of the atoms in the backbone of PhAcP. Such information is critical for the analysis of further NMR experiments to resolve the secondary conformation of PhAcP, as well as the folding state of PhAcP. The work involved is discussed in detail in the following sections.

3.3 Backbone resonance assignment of PhAcP in 50% (v/v) [EMIM][BF_4]

The sequential assignment strategy is based on a heteronuclear triple resonance approach making use of ^{15}N,^{13}C-labelled PhAcP (Ikura et al., 1990; Oh et al., 1988; Stockman et al., 1989). Three sets of paired experiments namely CBCA(CO)NH (Grzesiek & Bax, 1992a) and HNCACB (Wittekind & Mueller, 1993), HN(CO)CA (Bax & Ikura, 1991; Grzesiek & Bax, 1992b) and HNCA (Farmer et al., 1992; Grzesiek & Bax, 1992b; Kay et al., 1990), and HNCO (Grzesiek & Bax, 1992b; Kay et al., 1990; Muhandiram & Kay, 1994) and HN(CA)CO (Clubb et al., 1992) were acquired for one-bond correlations of backbone ^{1}H, ^{15}N and ^{13}C atoms and hence

sequential linkage patterns were obtained. For instance, in the first set of experiments, HNCACB correlates the backbone amide ^{1}H and ^{15}N resonance of a particular residue to the $^{13}C^{\beta}$ resonances of its own and preceding residue, thus providing information on the $^{13}C^{\alpha}$ and $^{13}C^{\beta}$ chemical shifts of a particular amino acid residue and its preceding residue. On the other hand, CBCA(CO)NH provides information on the $^{13}C^{\alpha}$ and $^{13}C^{\beta}$ chemical shifts of the preceding residue only by correlating an amide ^{1}H and ^{15}N resonances to the resonance of the preceding $^{13}C^{\beta}$. In this manner, the $^{13}C^{\alpha}$ and $^{13}C^{\beta}$ chemical shifts of a particular residue (i.e. a spin system) and its preceding one can be determined. Since each type of amino acid has its own characteristic range of $^{13}C^{\alpha}$ and $^{13}C^{\beta}$ chemical shifts, the possible types of amino acid of all spin systems can be deduced (Grzesiek & Bax, 1993). With the knowledge of the spin systems of own and preceding residue, together with the possible amino acid types of both residues, the spin systems are then linked by sequential connectivities (Figure 3.3) and fit into the primary sequence of the protein. As a result, all backbone amide resonances and $^{13}C^{\alpha}$ and $^{13}C^{\beta}$ resonances can be assigned unambiguously.

The set of CBCA(CO)NH and HNCACB experiments alone could not provide adequate information for an unambiguous sequential assignment of PhAcP in 50% (v/v) [EMIM][BF_4] mainly because the $^{13}C^{\alpha}$ resonance signals were sometimes

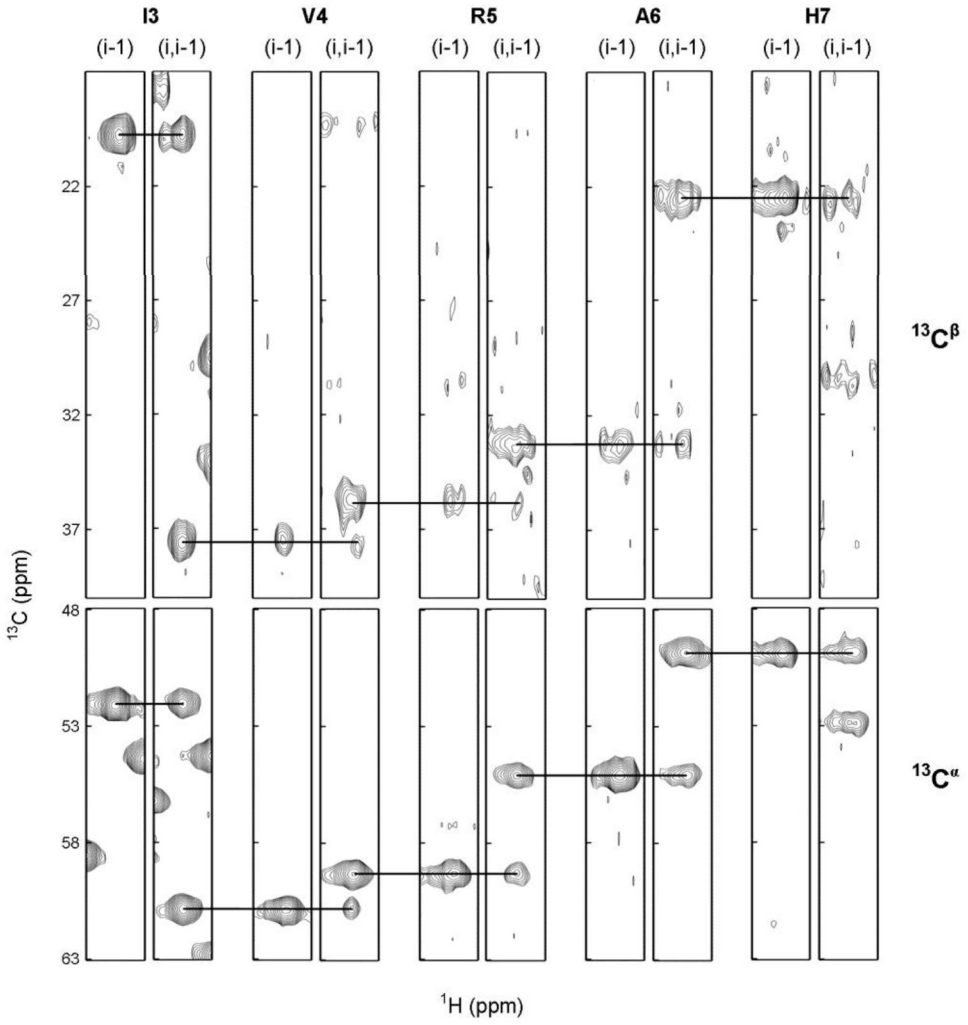

Figure 3.3. Main-chain sequential connectivities of residues Ile3 to His7 illustrated in selected pairs of ^{1}H-^{13}C strips from the 3D CBCA(CO)NH, HNCACB, HN(CO)CA and HNCA spectra of PhAcP in 50% (v/v) [EMIM][BF_4] at 298K and pH 5.3. Sequential connectivites are indicated by horizontal lines between strips. The upper panel contains spectra of CBCA(CO)NH and HNCACB. The left strip of each pair is taken from the CBCA(CO)NH spectrum which correlates the amide ^{1}H and ^{15}N resonances of a residue to the $^{13}C^{\beta}$ resonances of its preceding residue. The right strip of each pair is taken from the HNCACB spectrum which correlates the amide ^{1}H and ^{15}N resonances of a residue to the $^{13}C^{\beta}$ resonances of its own and its preceding residue. The lower panel contains spectra of HN(CO)CA and HNCA. The left strip of each pair is taken from the HN(CO)CA spectrum which correlates the amide ^{1}H and ^{15}N resonances of a residue to the $^{13}C^{\alpha}$ resonances of its preceding residue. The right strip of each pair is taken from the HNCA spectrum which correlates the amide ^{1}H and ^{15}N resonances of a residue to the $^{13}C^{\alpha}$ resonances of its own and its preceding residue.

too weak to be identified in the spectrum. Therefore, the second set of experiments, HN(CO)CA and HNCA, was acquired. These two experiments work in a similar manner to CBCA(CO)NH and HNCACB respectively but correlate amide resonances to $^{13}C^{\alpha}$ resonance only. Unfortunately, a significant number of residues had only the $^{13}C^{\alpha}$ resonance identified, while some residues even lost both the $^{13}C^{\alpha}$ and $^{13}C^{\beta}$ resonances. To cope with that, the third set of experiments, HNCO and HN(CA)CO, was employed to obtain additional information on the ^{13}CO resonance.

By the combination of all these triple resonance experiments, 62 out of 86 backbone amide resonances were successfully assigned as illustrated in the ^{1}H-^{15}N HSQC spectrum of PhAcP in 50% (v/v) [EMIM][BF_4] in Figure 3.4. The chemical shifts of $^{13}C^{\alpha}$, $^{13}C^{\beta}$, ^{13}CO, ^{15}N, H^{N} and H^{α} of each assigned residue are obtained and summarized in Table A1 in the Appendix.

3.4 Structural characterization of PhAcP in 50% (v/v) [EMIM][BF_4]

3.4.1 Secondary structure estimation by ^{13}C secondary shifts

With the knowledge of the $^{13}C^{\alpha}$ and $^{13}C^{\beta}$ chemical shifts of each residue from the backbone resonance assignment of PhAcP in 50% (v/v) [EMIM][BF_4], its

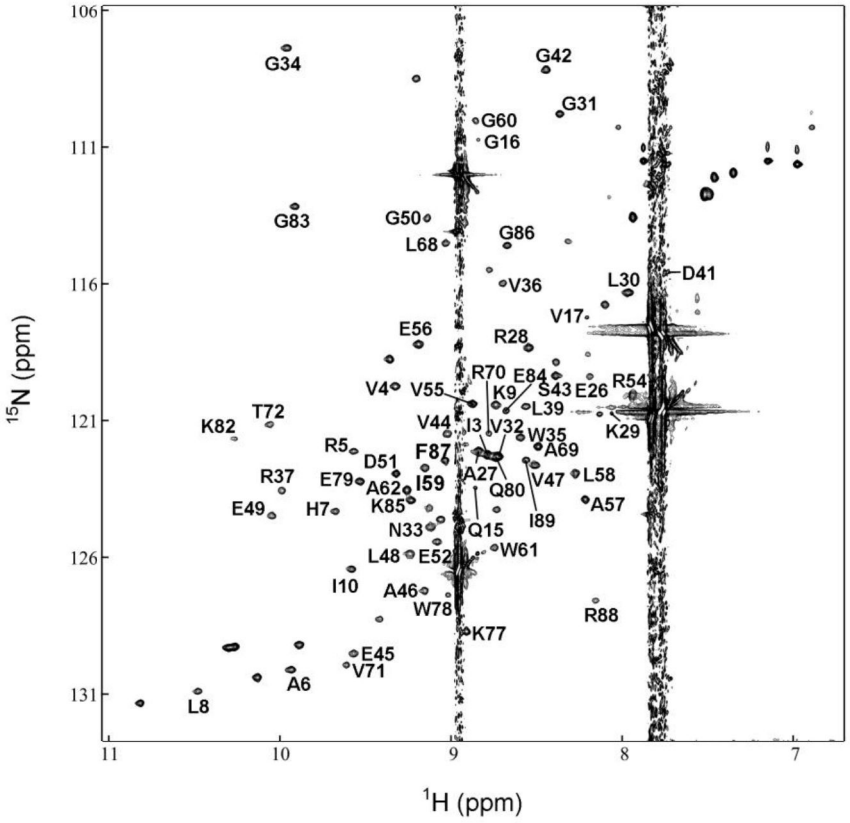

Figure 3.4. Backbone amide assignment of the ^{1}H-^{15}N HSQC spectrum of PhAcP in 50% (v/v) [EMIM][BF_4] at 298K and pH 5.3. The assignments of 62 backbone amide signals are indicated by the one-letter code and the residue number. There are still 24 unassigned peaks. 5 residues in the primary sequence (Met1, Pro40, Pro66, Pro67 and Pro81) do not produce amide peaks.

backbone secondary conformation can be estimated by the ^{13}C secondary shift of each residue (Spera & Bax, 1991; Wishart et al., 1991). Secondary shift is the deviation of the observed $^{13}C^{\alpha}$ and $^{13}C^{\beta}$ chemical shifts of a residue from the random coil chemical shifts of that particular type of amino acid. It is described by:

$$\Delta\Delta\delta_C = \Delta\delta_{C^\alpha} - \Delta\delta_{C^\beta} = (\delta_{C^\alpha(obs)} - \delta_{C^\alpha(rc)}) - (\delta_{C^\beta(obs)} - \delta_{C^\beta(rc)}) \quad (3)$$

where $\Delta\Delta\delta_C$ is the total secondary shift, $\Delta\delta_{C^\alpha}$ and $\Delta\delta_{C^\beta}$ are the secondary shifts of $^{13}C^{\alpha}$ and $^{13}C^{\beta}$, $\delta_{C^\alpha(obs)}$ and $\delta_{C^\beta(obs)}$ are the observed chemical shifts of $^{13}C^{\alpha}$ and $^{13}C^{\beta}$ of a residue, $\delta_{C^\alpha(rc)}$ and $\delta_{C^\beta(rc)}$ are the random coil chemical shifts of $^{13}C^{\alpha}$ and $^{13}C^{\beta}$ of that type of amino acid. The random coil chemical shift values used in this study (Table A2) are the average values from Biological Magnetic Resonance Data Bank (BMRB).

According to Spera and Bax (1991) and Wishart et al. (1991), the $^{13}C^{\alpha}$ and $^{13}C^{\beta}$ chemical shifts of a residue are affected by the secondary structure in which the residue is involved. For instance, the resonance of $^{13}C^{\alpha}$ shifts downfield (i.e. to a chemical shift of a larger value) for about 3 ppm on average when the residue is in an α-helical structure, but it shifts upfield in a β-sheet structure. On the contrary, the resonance of $^{13}C^{\beta}$ shows a very slight upfield shift in an α-helix but a significant downfield shift in a β-sheet. This results in a specific directional deviation of the $^{13}C^{\alpha}$

and $^{13}C^{\beta}$ chemical shifts from that when the residue is in a random coil, i.e. secondary shift. Equation (3) combines the $^{13}C^{\alpha}$ and $^{13}C^{\beta}$ secondary shifts, so that a residue in an α-helix is represented by a positive value, and a negative value defines a residue in a β-sheet structure.

The secondary structure of PhAcP in 50% (v/v) [EMIM][BF_4] was determined by the ^{13}C secondary shifts and compared with that observed in the absence of [EMIM][BF_4] (Figure 3.5). In 2005, Cheung and coworkers reported that the crystal structure of PhAcP in its native state consists of two α-helices and five β-strands as illustrated in Figure 3.5A as bars and arrows respectively. According to the ^{13}C chemical shifts data of PhAcP at 318K from Guan and coworkers (2005), the secondary shift (Figure 3.5B) reveals a secondary structure topology that agrees with what is observed in the crystal structure. Since the apparent T_m of PhAcP is 384.5K (Cheung et al., 2005), PhAcP in 318K adopts a native conformation. It implies that the native conformations of PhAcP observed in a crystal structure and an NMR solution structure are comparable. In Figure 3.5C, the ^{13}C chemical shifts of PhAcP in 50% (v/v) [EMIM][BF_4] indicates a similar secondary structure topology to the native state.

It is noted that the backbone resonance assignments of the residues Tyr11 to

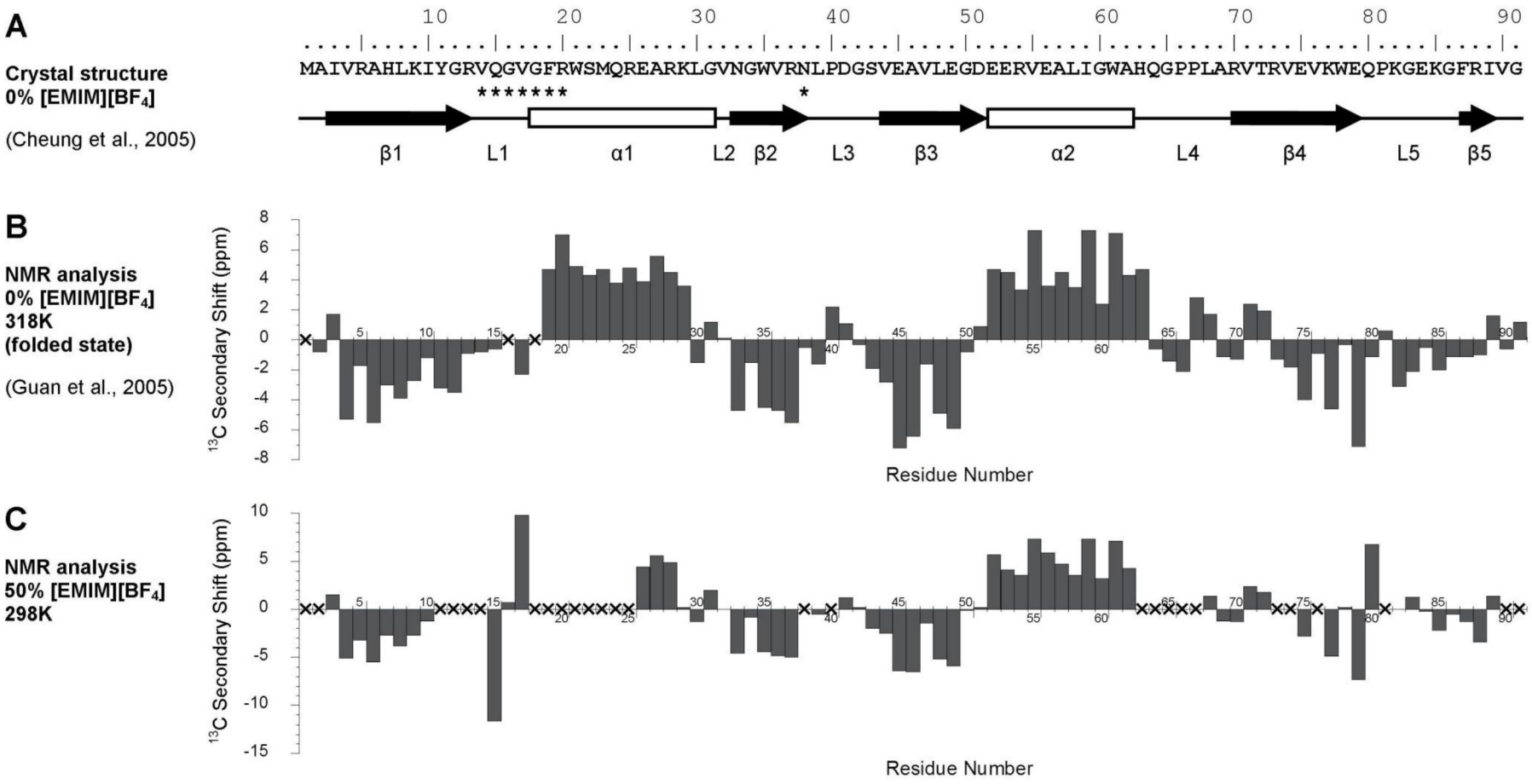

Figure 3.5. The secondary structure of PhAcP determined by ^{13}C secondary shifts in 50% (v/v) [EMIM][BF_4] at 298K and pH 5.3 generally matches its native secondary structure topology in the absence of ionic liquid observed in crystal structure and NMR

Figure 3.5. (Continued) spectroscopy. The top line shows the primary sequence of PhAcP. (A) The secondary structure of PhAcP observed in its crystal structure (Cheung et al., 2005). α-helices and β-strands are indicated by bars and arrows respectively. (B) The secondary structure determined from the ^{13}C secondary shifts in NMR spectroscopy at 318K (Guan et al., 2005). PhAcP is in folded state at this temperature according to its reported apparent T_m of 384.5K (Cheung et al., 2005). Positive bars indicate α-helices whereas negative bars indicate β-strands. Amino acid residues with unassigned $^{13}C^{\alpha}$ and $^{13}C^{\beta}$ are indicated by a cross (×) on the x-axis. (C) The secondary structure in 50% (v/v) [EMIM][BF_4] determined from the ^{13}C secondary shifts in NMR spectroscopy at 298K. The extreme secondary shifts in residues Gln15 and Val17 may imply interaction of the $[BF_4]^-$ ion with the PhAcP active site, which is denoted by an asterisk (*) in the primary sequence. The similarity of the three secondary structures suggests that PhAcP in 50% (v/v) [EMIM][BF_4] at 298K is in folded state adopting the native secondary structure topology.

Val14 and Gly18 to Arg25 are missing. Extreme secondary shifts are also found in residues Gln15 and Val17. Missing assignments and ill-defined secondary shift pattern infer an unstable chemical environment. Since the residues are in the active site region of PhAcP (Cheung et al., 2005), and the $[BF_4]^-$ ion of the ionic liquid resembles the phosphate group of acylphosphate, which is the primary substrate of PhAcP, the unstable chemical environment of the active site residues may suggest interaction of the $[BF_4]^-$ ion with the active site.

3.4.2 NOE connectivities within secondary structures

An additional independent proof of PhAcP adopting native secondary structure topology in 50% (v/v) [EMIM][BF_4] is the NOE connectivities within the secondary structures. In an ^1H-^{15}N NOESY-HSQC experiment (Bax et al., 1990; Frenkiel et al., 1990) that detects long-range NOE, the phenomenon of NOE occurs through space between an amide proton and all the other protons at a distance of < 5Å. The detection of such inter-proton NOE identifies the proximal amino acid residues for each residue. As a result, the relative position of all assigned residues can be deduced (Kumar et al., 1980).

In a β-sheet structure, H^N-H^α and H^N-H^N NOE connectivities can be observed between protons facing each other in adjacent strands (Figure 3.6A). Figure 3.6B summarizes the inter-strand H^N-H^α and H^N-H^N NOE connectivities observed in the part of PhAcP previously estimated to be in a β-sheet structure by ^{13}C secondary shifts. The NOE connectivities confirm the native-like five-β-strand secondary structure determined by ^{13}C secondary shifts. On top of that, the inter-strand NOE also infers that the β-sheet structure is composed of three pairs of anti-parallel strands and a pair of parallel strands as shown in Figure 3.6B. This topology agrees with that observed in the crystal structure of PhAcP in the absence of [EMIM][BF_4] (Cheung et al., 2005).

A characteristic NOE pattern in an α-helical structure is the H^N-H^N NOE between the amide protons of a residue (i) and its preceding (i–1) and succeeding (i+1) residues as demonstrated in Figure 3.7A. In the two α-helices previously determined by ^{13}C secondary shifts, the helical NOE pattern is observed in helix-2 and the C-terminus of helix-1. It serves as an alternative proof to the two native-like helical structures of PhAcP in 50% (v/v) [EMIM][BF_4], leaving uncertainty only to the N-terminus of helix-1 with unknown NOE due to unsuccessful backbone assignment.

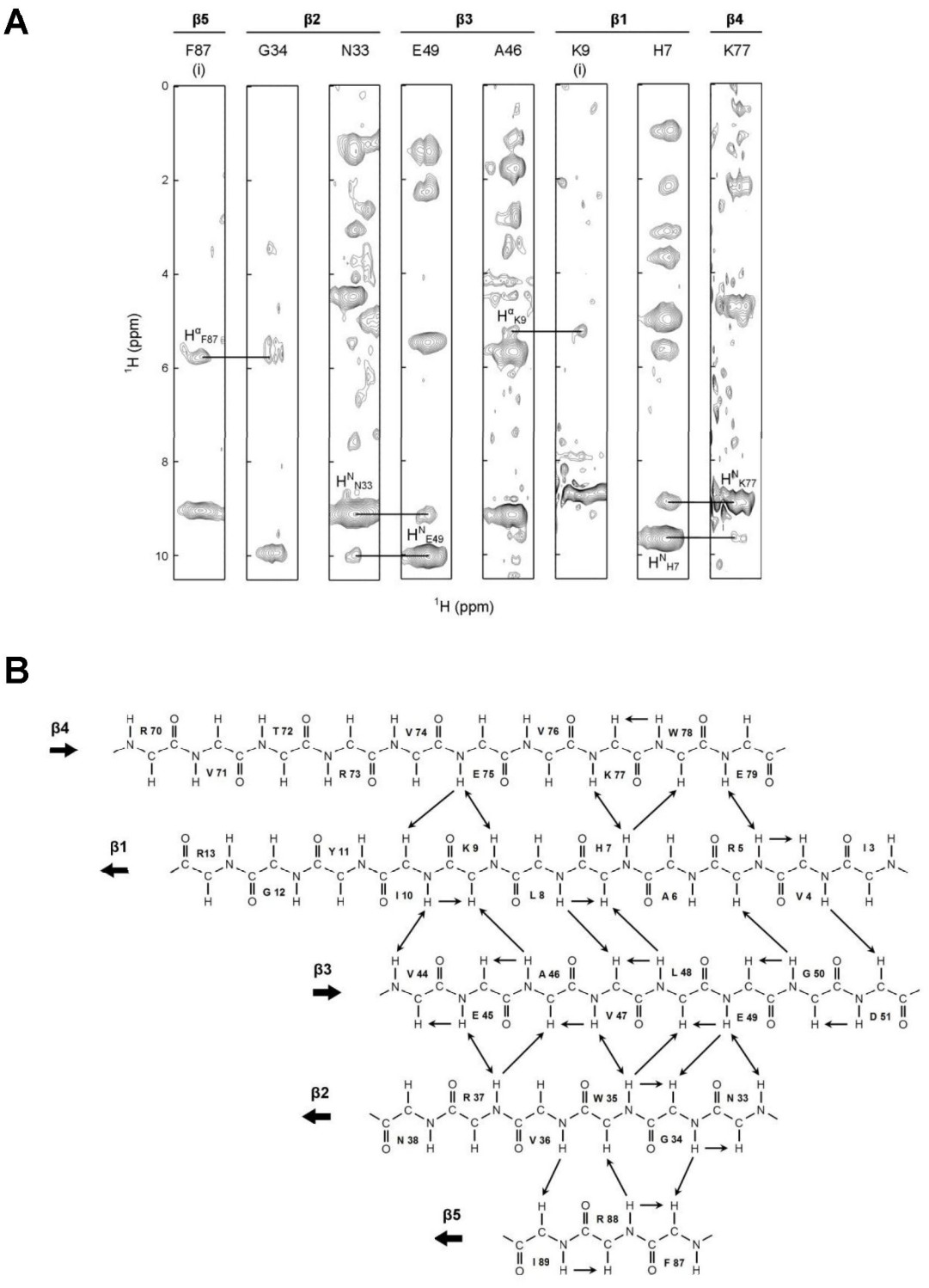

Figure 3.6. H^N-H^{α} and H^N-H^N NOE connectivities of residues facing each other in adjacent strands in the β-sheet structure of PhAcP in 50% (v/v) [EMIM][BF_4]. (A) Selected pairs of adjacent residues in the β-sheet illustrate their NOE connectivities in their respective ^{1}H-^{1}H strips from the 3D ^{15}N-TOCSY-HSQC and ^{1}H-^{15}N NOESY-HSQC spectra of PhAcP in 50% (v/v) [EMIM][BF_4] at 298K and

Figure 3.6. (Continued) pH 5.3. Connectivites are indicated by horizontal lines between strips. Strips denoted by "(i)" are taken from the ^{15}N-TOCSY-HSQC spectrum which correlates the amide ^{1}H and ^{15}N resonances of a residue to all ^{1}H resonances of its own. The ^{1}H-^{15}N NOESY-HSQC spectrum correlates the amide resonances to the resonances of all ^{1}H in close proximity, including those of its own. (B) A summary of all H^N-H^α and H^N-H^N NOE connectivities observed in the β-sheet structure of PhAcP in 50% (v/v) [EMIM][BF_4]. The inter-strand NOE connectivities suggest a native-like five-β-strand structure with three pairs of anti-parallel strands and a pair of parallel strands.

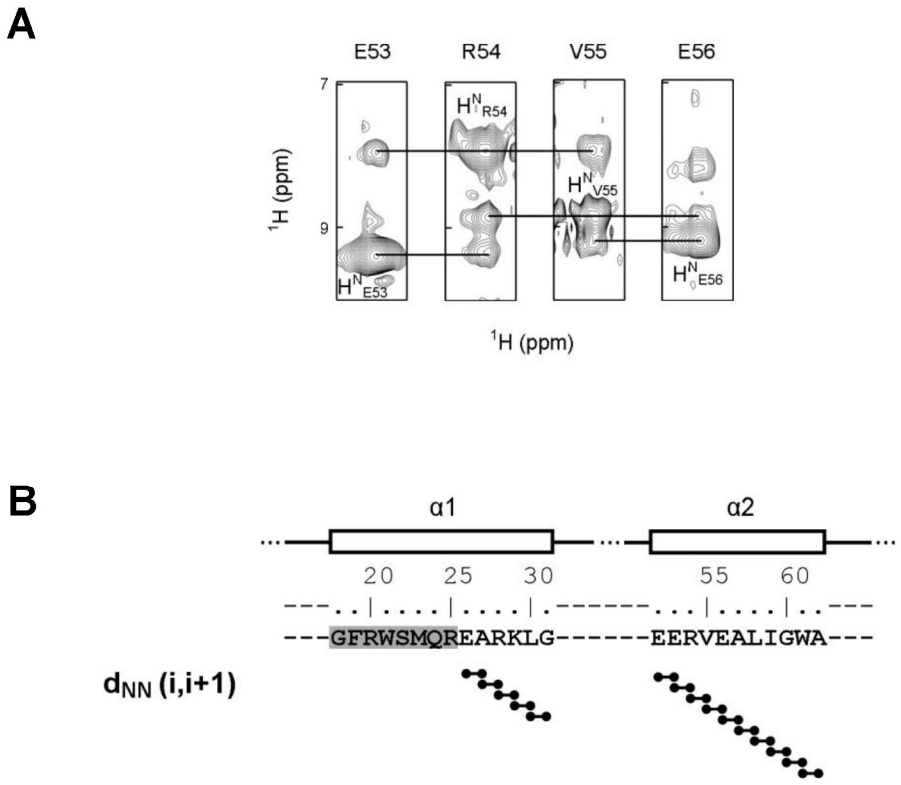

Figure 3.7. H^N-H^N NOE connectivities of consecutive residues in the α-helical structure of PhAcP in 50% (v/v) [EMIM][BF_4]. (A) Residues Glu53 to Glu56 in helix-2 illustrate their NOE connectivities in their respective ^{1}H-^{1}H strips from the 3D ^{1}H-^{15}N NOESY-HSQC spectrum of PhAcP in 50% (v/v) [EMIM][BF_4] at 298K and pH 5.3. Connectivites are indicated by horizontal lines between strips. The ^{1}H-^{15}N NOESY-HSQC spectrum correlates the amide ^{1}H and ^{15}N resonances of a residue to the resonances of all ^{1}H in close proximity, including those of its own. In an α-helical structure, $^1H^N$ resonances of its own, preceding and succeeding residues are generally observed. (B) A summary of all H^N-H^N NOE connectivities observed in the α-helical structures of PhAcP in 50% (v/v) [EMIM][BF_4]. The top line shows the part of primary sequence of PhAcP containing the α-helical structures and the two α-helices are indicated by separate bars. Residues unable to be assigned in the ^{1}H-^{15}N HSQC spectrum are shaded in grey. H^N-H^N NOE transfer in a distance of one residue away is indicated by horizontal lines. Except for the unassigned N-terminus of helix-1, helical NOE pattern is observed in both helices.

In conclusion, NOE is observed within the secondary structures determined by the ^{13}C secondary shifts. The agreement of the two approaches strongly indicates that the backbone secondary conformation of PhAcP in 50% (v/v) [EMIM][BF_4] resembles the native topology. In essence, it consists of two α-helices and five β-strands arranged into three pairs of anti-parallel strands and a pair of parallel strands.

3.5 Characterization of the conformational stability of PhAcP in 50% (v/v) [EMIM][BF_4] by guanidine thiocyanate-induced denaturation

The conformational stability of PhAcP in both the absence and presence of 50% (v/v) [EMIM][BF_4] was determined by guanidine thiocyanate (GdnSCN)-induced denaturation from which the mid-point of transition value ($[GdnSCN]_{1/2}$) was obtained. $[GdnSCN]_{1/2}$ is the concentration of guanidine thiocyanate at which half the amount of PhAcP in the sample is denatured. Therefore, a higher $[GdnSCN]_{1/2}$ indicates a higher stability of PhAcP against denaturation.

The approach to follow the denaturation of PhAcP was the 2D ^{1}H-^{15}N HSQC experiment (Bodenhausen & Ruben, 1980). A series of 2D ^{1}H-^{15}N HSQC experiment

was acquired for PhAcP with an increasing concentration of guanidine thiocyanate. With reference to the illustration in Figure 3.8, when PhAcP is progressively denatured by guanidine thiocyanate, the intensities of the amide resonances representing the amino acid residues of native PhAcP drop. Meanwhile, amide signals indicating the residues of unfolded PhAcP appear gradually at a confined region near the centre of the spectrum as the unfolded residues are exposed to the solvent which is an identical chemical environment. Therefore, the reduction in the native resonance intensities, which indicates the relative amount of native PhAcP, can serve as a probe to follow the unfolding of PhAcP. With the previous backbone amide assignment of native PhAcP in 0% (Guan et al., 2005) and 50% (v/v) [EMIM][BF_4], the well-resolved native resonances can be identified and monitored upon denaturation by guanidine thiocyanate. The intensities of the traceable amide resonances are estimated and summed up to reduce error. The total intensity is then converted into a fraction indicating the relative amount of unfolded PhAcP in the sample (i.e. fraction unfolded). In this manner, the denaturation of PhAcP should result in a denaturation curve as shown in the schematic diagram in Figure 3.8. By fitting the data into a two-state model (Santoro & Bolen, 1988), the value of $[GdnSCN]_{1/2}$, which is a measure of PhAcP stability, can be obtained.

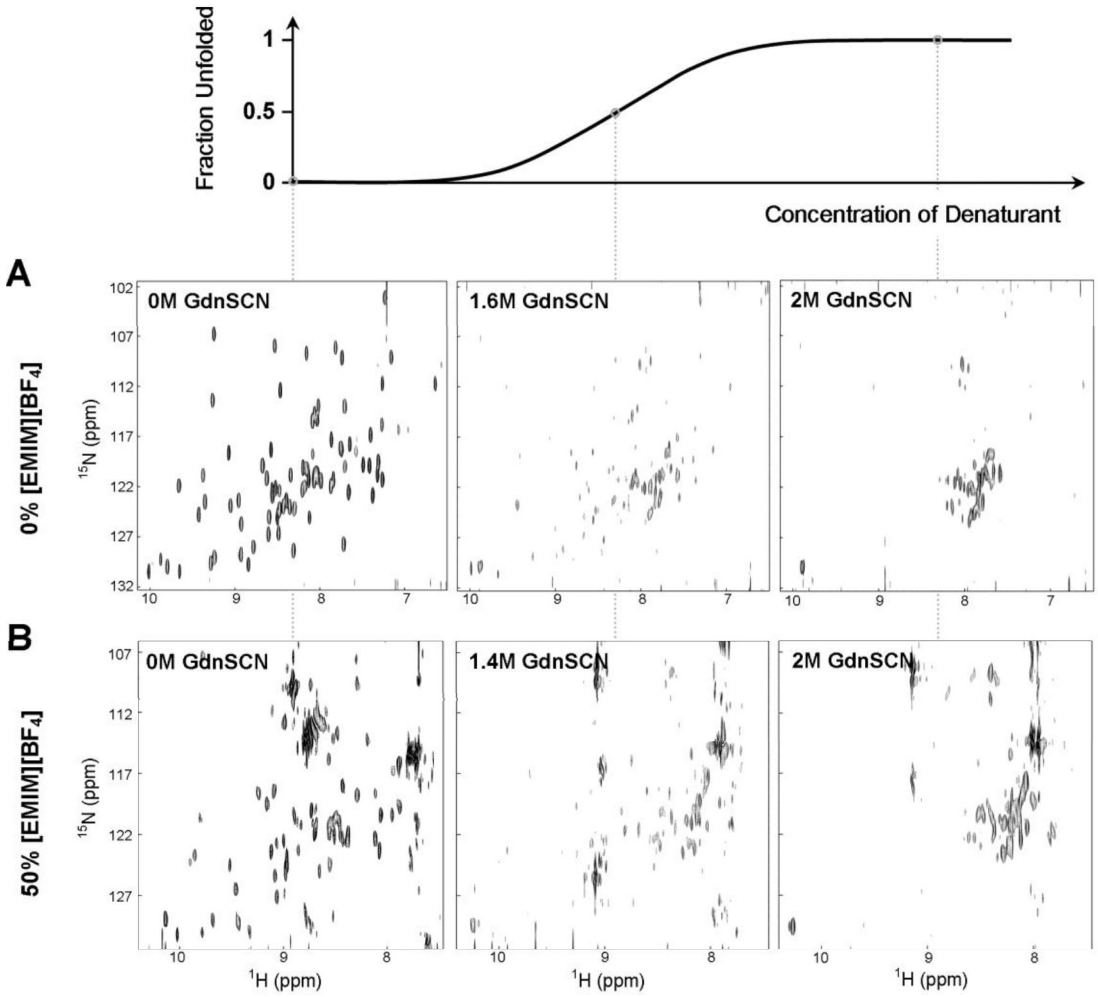

Figure 3.8. Guanidine thiocynate-induced denaturation of PhAcP can be followed by the disappearance of amide resonances of native PhAcP in the ^{1}H-^{15}N HSQC spectra. In both conditions with (A) no [EMIM][BF_4] and (B) 50% (v/v) [EMIM][BF_4], as the concentration of guanidine thiocyanate increases, the amide resonances of native PhAcP disappear while that of unfolded PhAcP appear gradually. The middle spectra contain amide signals from both the native and denatured states. Therefore, the reduction in native peak intensities can serve as a probe to follow the unfolding of PhAcP. The above spectra were obtained at 338K.

Guanidine thiocyanate-induced denaturation was performed at three temperatures, namely 318K, 328K and 338K, and the denaturation curves and $[GdnSCN]_{1/2}$ of PhAcP in the absence or presence of 50% (v/v) $[EMIM][BF_4]$ are summarized in Figure 3.9. In Figure 3.9A, at all the three temperature the two denaturation curves representing PhAcP in the absence or presence of 50% (v/v) $[EMIM][BF_4]$ closely overlap with each other. The similar $[GdnSCN]_{1/2}$ values obtained from the curves (Figure 3.9B) also reveal no observable trend that 50% (v/v) $[EMIM][BF_4]$ has any effect on the stability of PhAcP.

Despite the presence of 50% (v/v) $[EMIM][BF_4]$, the stability of PhAcP decreases as a function of temperature as indicated by a left-shift of the denaturation curves and a consistent decrease in the $[GdnSCN]_{1/2}$ values. It indicates the thermal denaturation of PhAcP and thus proves the validity of the 2D NMR assay to follow the denaturation of PhAcP.

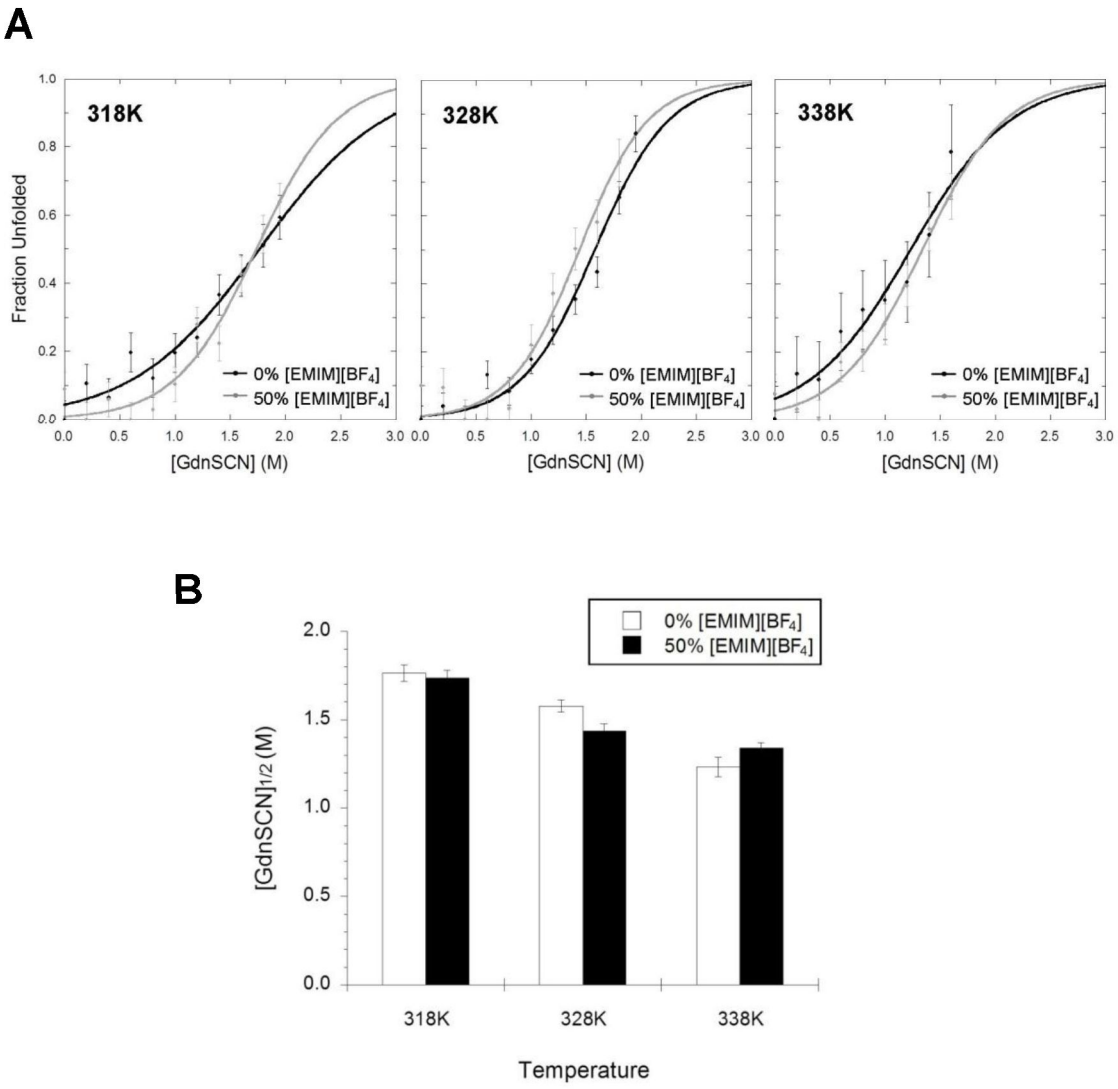

Figure 3.9. The denaturation curves and $[GdnSCN]_{1/2}$ of PhAcP determined by guanidine thiocyanate-induced denaturation in 0% and 50% (v/v) [EMIM][BF_4] at 318K, 328K and 338K. (A) The two denaturation curves representing PhAcP in the absence (black) or presence (grey) of 50% (v/v) [EMIM][BF_4] closely overlap with each other at 318K, 328K and 338K. This plot shows a fraction unfolded parameter converted from the sum of amide resonance intensities of 27-42 residues in the ^{1}H-^{15}N HSQC spectra that were traceable upon denaturation. The error bars are estimated from the noise of the spectra. Curve-fitting is based on the observation that PhAcP can be completely denatured at high concentration of guanidine thiocyanate, at which no native amide signal can be identified in the spectra to produce a data point. (B) The $[GdnSCN]_{1/2}$ values obtained from the denaturation curves are similar despite the presence of 50% (v/v) [EMIM][BF_4], suggesting no observable trend that 50% (v/v) [EMIM][BF_4] has any effect on the stability of PhAcP. The consistent

Figure 3.9. (Continued) decrease in $[GdnSCN]_{1/2}$ as a function of temperature indicates thermal denaturation of PhAcP and proves the validity of the assay. The $[GdnSCN]_{1/2}$ values of PhAcP in the absence of $[EMIM][BF_4]$ at 318K, 328K and 338K are 1.76 ± 0.05 M, 1.58 ± 0.03 M and 1.23 ± 0.06 M respectively; while that in 50% (v/v) $[EMIM][BF_4]$ are 1.74 ± 0.04 M, 1.44 ± 0.04 M and 1.34 ± 0.03 M respectively. The error bars denote curve-fitting errors.

Chapter 4 Discussion

4.1 The structure of PhAcP in 50% (v/v) [EMIM][BF_4] resembles the native conformation

The ^{13}C secondary shifts and the NOE connectivities were used to determine the secondary structure of PhAcP in 50% (v/v) [EMIM][BF_4] and both approaches indicate the resemblance of the backbone secondary conformation of PhAcP in 50% (v/v) [EMIM][BF_4] to the native topology. In particular, the ^{13}C secondary shifts suggest a native-like secondary structure consisting of two α-helices and five β-strands, while the NOE connectivities support such topology and the inter-strand NOE infers that the β-sheet structure is composed of three pairs of anti-parallel strands and a pair of parallel strands as in the native conformation. These observations suggest that PhAcP has secondary structures arranged in native-like topology and there is no major alteration in the tertiary structure.

4.2 The conformational stability of PhAcP has no observable change in 50% (v/v) [EMIM][BF_4]

Guanidine thiocyanate-induced denaturation was performed at 318K, 328K and 338K to investigate the conformational stability of PhAcP in 50% (v/v) [EMIM][BF_4] and the denaturation of PhAcP was probed by 2D ^{1}H-^{15}N HSQC experiments in which the intensities of the amide resonances of residues in native PhAcP correspond to the amount of native PhAcP in the sample. Denaturation curves and the $[GdnSCN]_{1/2}$ values, that represent the concentration of guanidine thiocyanate at which half the amount of PhAcP in the sample is denatured, were obtained.

The stability of PhAcP is not altered in the presence of 50% (v/v) [EMIM][BF_4], as indicated by the closely overlapping denaturation curves and the similar $[GdnSCN]_{1/2}$ values consistently at the three temperatures of 318K, 328K and 338K. It is also noted that the stability of PhAcP decreases as a function of temperature despite the presence of 50% (v/v) [EMIM][BF_4]. It indicates thermal denaturation of PhAcP and proves the validity of the 2D NMR approach to probe for PhAcP denaturation.

4.3 Insight into the application of enzyme in ionic liquid

This study presents a high-resolution proof of the absence of adverse effect of 50% (v/v) [EMIM][BF_4] on the structure and the conformational stability of PhAcP. Unlike previous studies that investigate the protein structure in ionic liquid with indirect probes including intrinsic fluorescence (De Diego et al., 2005) and circular dichroism (Bihari et al., 2010; De Diego et al., 2004, 2005; Sasmal et al., 2011; Sen Mojumdar et al., 2012), the use of 2D and 3D NMR spectroscopy in this study enables the protein structure to be observed at atomic level and thus provides direct evidence to the absence of major protein structural alteration in ionic liquid. As for protein stability, it is previously described by the residual enzymatic activity over incubation time (De Diego et al., 2004, 2005; De Los Ríos et al., 2007; Ebrahimi et al., 2012; Ha et al., 2008; Noritomi et al., 2011), which is actually a complex function of protein and substrate solubility, protein conformation and reaction yield. The approach of NMR to detect the loss of protein conformation upon guanidine thiocyanate-induced denaturation in this study, on the other hand, directly addresses the conformational stability of the protein against denaturation. In addition, it allows the stability study of protein with no enzymatic activity, as well as the study of protein behavior in ionic liquids with strong UV absorption that poses interference

for conventional protein assays. In these circumstances, the method involving NMR spectroscopy demonstrated here is shown advantageous in future characterizations of protein structure and stability in ionic liquid in detail.

The application of [EMIM][BF_4] in industrial biocatalysis and research in protein science that require native protein properties is encouraged since [EMIM][BF_4] has a high potential for causing no destruction to the structure and stability of proteins based on the observations that the native basic structure and conformational stability of PhAcP are retained in the presence of 50% (v/v) [EMIM][BF_4].

4.4 Limitation of the study

The enzymatic activity of PhAcP in [EMIM][BF_4] is not characterized due to the resemblance of the $[BF_4]^-$ ion to the phosphate group of acylphosphate which is the primary substrate of PhAcP. The interaction between the $[BF_4]^-$ ion and the active site of PhAcP is suggested by the extreme ^{13}C secondary shifts of residues Gln15 and Val17 in the active site as well as the consistent missing backbone resonance assignment of the residues in the active site. As the $[BF_4]^-$ ion is a possible inhibitor

of PhAcP, it is infeasible to determine the enzymatic activity of PhAcP in [EMIM][BF_4].

4.5 Insight into future studies

The present study addresses the structure and conformational stability of PhAcP in 50% (v/v) [EMIM][BF_4] at a high resolution with the NMR technique. The characterization approach involved opens the door for further studies on the structure and stability of different classes of protein as a function of ionic liquid concentration or ionic liquid composition in a more systematic way. Such studies may eventually provide insight into the general effect of ionic liquid to the protein folding energetics.

Chapter 5 Conclusions

This study demonstrated the application of NMR spectroscopy to characterize the structure and conformational stability of PhAcP in 50% (v/v) [EMIM][BF_4]. As the first step, 62 out of 86 backbone amide resonances were successfully assigned for the chemical shifts of $^{13}C^{\alpha}$, $^{13}C^{\beta}$, ^{13}CO, ^{15}N, H^N and H^{α} of each assigned residue. The backbone assignment was based on three sets of triple resonance experiments, namely CBCA(CO)NH and HNCACB, HN(CO)CA and HNCA, and HNCO and HN(CA)CO.

The secondary structure of PhAcP in 50% (v/v) [EMIM][BF_4] was then determined by the ^{13}C secondary shift and their spatial arrangement was further confirmed by the NOE connectivities within the secondary structures. The evidence from the two approaches indicate that the secondary structural arrangement of PhAcP in 50% (v/v) [EMIM][BF_4] resembles the native topology, which consists of two α-helices and five β-strands arranging into three pairs of anti-parallel strands and a pair of parallel strands. Therefore, there is no major change in its tertiary structure.

The conformational stability of PhAcP in 50% (v/v) [EMIM][BF_4] was investigated by guanidine thiocyanate-induced denaturation monitored by 2D

^{1}H-^{15}N HSQC experiments at 318K, 328K and 338K. From the comparison of the denaturation curves and $[GdnSCN]_{1/2}$ values obtained, there is no observable effect of 50% (v/v) $[EMIM][BF_4]$ on the stability of PhAcP.

Appendix

Table A1. The ^{1}H, ^{15}N and ^{13}C assignment for PhAcP in 50% (v/v) [EMIM][BF_4] at 298K and pH 5.3.

Amino acid residues	Chemical shift (ppm)					
	$^{13}C^{\alpha}$	$^{13}C^{\beta}$	^{13}CO	^{15}N	H^{N}	H^{α}
M 1	—	—	—	—	—	—
A 2	—	—	—	—	—	—
I 3	60.875	37.656	176.049	122.254	8.778	—
V 4	59.319	35.808	173.899	119.754	9.313	5.326
R 5	55.116	33.450	173.343	122.119	9.564	4.810
A 6	49.859	22.542	175.081	130.110	9.913	6.056
H 7	52.918	30.422	174.371	124.318	9.663	5.618
L 8	54.685	46.519	—	130.903	10.474	—
K 9	56.970	36.297	174.706	120.420	8.719	5.208
I 10	61.821	41.283	174.041	126.428	9.547	4.810
Y 11	—	—	—	—	—	—
G 12	—		—	—	—	—
R 13	—	—	—	—	—	—
V 14	—	—	—	—	—	—
Q 15	56.319	41.792	175.795	123.468	8.892	5.088
G 16	45.939		174.633	110.738	8.861	—
V 17	67.090	28.722	—	117.244	8.198	—
G 18	—		—	—	—	—
F 19	—	—	—	—	—	—
R 20	—	—	—	—	—	—
W 21	—	—	—	—	—	—
S 22	—	—	—	—	—	—
M 23	—	—	—	—	—	—
Q 24	—	—	—	—	—	—
R 25	—	—	—	—	—	—
E 26	58.524	28.081	178.292	119.388	8.166	—
A 27	56.216	17.772	180.749	122.118	8.815	—
R 28	59.874	30.117	180.067	118.341	8.582	—
K 29	—	32.648	178.524	120.740	8.031	—
L 30	55.486	44.827	177.648	116.320	7.930	4.594
G 31	47.173		174.817	109.790	8.368	—

Table 1. (Continued)

Amino acid residues	Chemical shift (ppm)					
	$^{13}C^{\alpha}$	$^{13}C^{\beta}$	^{13}CO	^{15}N	H^{N}	H^{α}
V 32	62.847	34.198	174.393	122.334	8.689	4.420
N 33	52.566	43.110	174.484	124.896	9.110	5.466
G 34	44.428		171.941	107.381	9.941	5.442
W 35	54.756	32.303	174.467	121.610	8.576	5.402
V 36	59.672	35.919	172.465	115.985	8.698	—
R 37	55.076	35.162	174.290	123.564	9.961	5.626
N 38	—	—	—	—	—	—
L 39	—	42.978	178.775	120.490	8.537	5.556
P 40	—	—	—	—		—
D 41	53.906	40.153	—	115.605	7.748	—
G 42	45.432		174.512	108.177	8.422	—
S 43	58.565	66.573	174.069	119.363	8.391	5.138
V 44	61.775	35.673	—	121.495	8.998	5.085
E 45	53.695	34.108	174.201	129.523	9.549	5.615
A 46	50.888	24.630	174.913	127.222	9.157	5.670
V 47	61.495	34.273	173.744	122.635	8.510	5.573
L 48	52.973	46.201	175.303	125.870	9.235	5.518
E 49	55.148	35.027	175.650	124.477	10.032	6.282
G 50	45.139		171.804	113.614	9.161	4.828
D 51	56.135	43.346	178.539	122.944	9.293	4.814
E 52	61.360	29.697	177.265	125.438	9.098	4.409
E 53	60.368	—	179.623	118.766	9.413	4.555
R 54	58.780	30.316	178.516	120.095	7.912	4.541
V 55	68.258	32.314	—	120.387	8.866	—
E 56	60.194	28.311	179.624	118.210	9.201	4.561
A 57	55.729	18.214	181.051	123.887	8.186	—
L 58	57.616	42.048	179.252	122.938	8.247	—
I 59	67.251	38.252	180.066	122.735	9.149	—
G 60	48.350		—	110.034	8.824	—
W 61	62.801	28.773	178.894	125.639	8.742	—
A 62	55.000	17.901	175.423	123.546	9.235	—
H 63	—	—	—	—	—	—
Q 64	—	—	—	—	—	—
G 65	—		—	—	—	—
P 66	—	—	—	—		—

Table 1. (Continued)

Amino acid residues	Chemical shift (ppm)					
	$^{13}C^{\alpha}$	$^{13}C^{\beta}$	^{13}CO	^{15}N	H^{N}	H^{α}
P 67	—	—	—	—		—
L 68	55.558	42.156	—	114.519	9.057	—
A 69	52.463	20.832	—	121.960	8.488	4.924
R 70	55.095	31.475	—	121.478	8.777	5.010
V 71	63.765	—	177.967	129.939	9.593	—
T 72	62.650	69.645	—	121.150	10.045	—
R 73	—	—	—	—	—	—
V 74	—	—	—	—	—	—
E 75	55.331	32.153	175.698	129.211	9.867	5.099
V 76	—	—	—	—	—	—
K 77	54.914	36.419	—	128.714	8.884	4.969
W 78	57.336	30.235	176.848	127.372	9.065	5.089
E 79	54.368	35.641	175.603	123.211	9.522	5.360
Q 80	62.500	29.567	—	122.325	8.748	—
P 81	—	—	—	—		—
K 82	56.229	—	—	121.662	10.267	—
G 83	46.546		175.482	113.175	9.891	—
E 84	56.595	30.807	176.778	120.653	8.671	—
K 85	56.129	34.961	—	123.914	9.234	4.926
G 86	44.734		172.184	114.604	8.664	—
F 87	57.528	41.805	175.803	122.458	9.036	5.756
R 88	55.458	33.935	174.727	127.585	8.160	5.318
I 89	62.069	38.967	177.232	122.439	8.553	—
V 90	—	—	—	—	—	—
G 91	—		—	—	—	—

* Missing assignments are indicated by a deletion line (—).

Table A2. The ^{13}C random coil chemical shifts (in ppm) of the 20 common amino acids. (average values from BMRB)

Amino acid		$^{13}C^{\alpha}$	$^{13}C^{\beta}$
A	Ala	52.1	19.3
C	Cys	58.2 (reduced)	29.4 (reduced)
		55.3 (oxidized)	40.5 (oxidized)
D	Asp	53.8	41.2
E	Glu	56.3	30.3
F	Phe	57.2	40.2
G	Gly	45.2	—
H	His	55.3	30.1
I	Ile	60.4	38.7
K	Lys	56.2	32.8
L	Leu	54.5	42.5
M	Met	55.4	33.7
N	Asn	53.0	38.9
P	Pro	62.6	31.9
Q	Gln	55.5	29.4
R	Arg	55.9	31.0
S	Ser	58.1	64.1
T	Thr	60.9	69.7
V	Val	61.4	32.8
W	Trp	57.3	30.4
Y	Tyr	57.6	39.4

References

Arai, S., Nakashima, K., Tanino, T., Ogino, C., Kondo, A., & Fukuda, H. (2010). Production of biodiesel fuel from soybean oil catalyzed by fungus whole-cell biocatalysts in ionic liquids. *Enzyme and Microbial Technology, 46*(1), 51-55.

Baker, S. N., McCleskey, T. M., Pandey, S., & Baker, G. A. (2004). Fluorescence studies of protein thermostability in ionic liquids. *Chemical Communications,* (8), 940-941.

Barrera-Rivera, K. A., Marcos-Fernández, Á., Vera-Graziano, R., & Martínez-Richa, A. (2009). Enzymatic ring-ppening polymerization of ε-caprolactone by *Yarrowia lipolytica* lipase in ionic liquids. *Journal of Polymer Science: Part A: Polymer Chemistry, 47*(21), 5792-5805.

Bax, A., & Ikura, M. (1991). An efficient 3D NMR technique for correlating the proton and ^{15}N backbone amide resonances with the α-carbon of the preceding residue in uniformly $^{15}N/^{13}C$ enriched proteins. *Journal of Biomolecular NMR, 1*(1), 99-104.

Bax, A., Ikura, M., Kay, L. E., Torchia, D. A., & Tschudin, R. (1990). Comparison of different modes of two-dimensional reverse-correlation NMR for the study of proteins. *Journal of Magnetic Resonance, 86*(2), 304-318.

Bekhouche, M., Blum, L. J., & Doumèche, B. (2012). Contribution of dynamic and static quenchers for the study of protein conformation in ionic liquids by steady-state fluorescence spectroscopy. *The Journal of Physical Chemistry B, 116*(1), 413-423.

Bihari, M., Russell, T. P., & Hoagland, D. A. (2010). Dissolution and dissolved state of cytochrome c in a neat, hydrophilic ionic liquid. *Biomacromolecules, 11*(11), 2944-2948.

Bodenhausen, G., & Ruben D. J. (1980). Natural abundance nitrogen-15 NMR by enhanced heteronuclear spectroscopy. *Chemical Physics Letters, 69*(1), 185-189.

Carmichael, A. J., & Seddon, K. R. (2000). Polarity study of some 1-alkyl-3-methylimidazolium ambient-temperature ionic liquids with the solvatochromic dye, Nile Red. *Journal of Physical Organic Chemistry, 13*(10), 591-595.

Cheung, Y. Y., Lam, S. Y., Chu, W. K., Allen, M. D., Bycroft, M., & Wong, K. B. (2005). Crystal structure of a hyperthermophilic archaeal acylphosphatase from *Pyrococcus horikoshii* – Structural insights into enzymatic catalysis, thermostability, and dimerization. *Biochemistry, 44*(12), 4601-4611.

Clubb, R. T., Thanabal, V., & Wagner, G. (1992) A constant-time three-dimensional triple-resonance pulse scheme to correlate intraresidue $^{1}H^{N}$, ^{15}N, and $^{13}C'$ chemical shifts in ^{15}N-^{13}C-labeled proteins. *Journal of Magnetic Resonance, 97*(1), 213-217.

Constantinescu, D., Weingärtner, H., & Herrmann, C. (2007). Protein dnaturation by ionic liquids and the Hofmeister series: A case study of aqueous solutions of ribonuclease A. *Angewandte Chemie International Edition, 46*(46), 8887-8889.

De Diego, T., Lozano, P., Gmouh, S., Vaultier, M., & Iborra, J. L. (2004). Fluorescence and CD spectroscopic analysis of the α-chymotrypsin stabilization by the ionic liquid, 1-ethyl-3-methylimidazolium bis [(trifluoro-methyl) sulfonyl] amide. *Biotechnology and Bioengineering, 88*(7), 916-924.

De Diego, T., Lozano, P., Gmouh, S., Vaultier, M., & Iborra, J. L. (2005). Understanding structure-stability relationships of *Candida antartica* lipase B in ionic liquids. *Biomacromolecules, 6*(3), 1457-1464.

Delaglio, F., Grzesiek, S., Vuister, G. W., Zhu, G., Pfeifer, J., & Bax, A. (1995). NMRPipe: A multidimensional spectral processing system based on UNIX pipes. *Journal of Biomolecular NMR, 6*(3), 277-293.

De Los Ríos, A. P., Hernández-Fernández, F. J., Martínez, F. A., Rubio, M., & Víllora, G. (2007). The effect of ionic liquid media on activity, selectivity and stability of *Candida antarctica* lipase B in transesterification reactions. *Biocatalysis and Biotransformation, 25*(2-4), 151-156.

Ebrahimi, M., Hosseinkhani, S., Heydari, A., Khavari-Nejad, R. A., & Akbari, J. (2012). Improvement of thermostability and activity of firefly luciferase through [TMG][Ac] ionic liquid mediator. *Applied Biochemistry and Biotechnology, 168*(3), 604-615.

Erbeldinger, M., Mesiano, A. J., & Russell, A. J. (2000). Enzymatic catalysis of formation of Z-aspartame in ionic liquid − An alternative to enzymatic catalysis in organic solvents. *Biotechnology Progress, 16*(6), 1129-1131.

Farmer, B. T., Venters, R. A., Spicer, L. D., Wittekind, M. G., & Müller, L. (1992) A refocused and optimized HNCA: Increased sensitivity and resolution in large macromolecules. *Journal of Biomolecular NMR, 2*(2), 195-202.

Frenkiel, T., Bauer, C., Carr, M. D., Birdsall, B., & Feeney, J. (1990) HMQC-NOESY-HMQC, a three-dimensional NMR experiment which allows detection of nuclear Overhauser effects between protons with overlapping signals. *Journal of Magnetic Resonance, 90*(2), 420-425.

Fujita, K., MacFarlane, D. R., & Forsyth M. (2005). Protein solubilising and stabilising ionic liquids. *Chemical Communications,* (38), 4804-4806.

Grzesiek, S., & Bax, A. (1992a). Correlating backbone amide and side chain resonances in larger proteins by multiple relayed triple resonance NMR. *Journal of the American Chemical Society, 114*(16), 6291-6293.

Grzesiek, S., & Bax, A. (1992b). Improved 3D triple-resonance NMR techniques applied to a 31 kDa protein. *Journal of Magnetic Resonance, 96*(2), 432-440.

Grzesiek, S., & Bax, A. (1993). Amino acid type determination in the sequential assignment procedure of uniformly $^{13}C/^{15}N$-enriched proteins. *Journal of Biomolecular NMR, 3*(2), 185-204.

Guan, X., Tse, M. K., Yang, Y., Sze, K. H., Cheung, K. K., & Wong, K. B. (2005, April 23). *Structure and dynamics of a thermophilic acylphosphatase from Pyrococcus horikoshii by NMR spectroscopy: Structural basis of thermostability and enzymatic activities*. Paper presented at the 12th Symposium on Chemistry Postgraduate Research in Hong Kong, Hong Kong.

Ha, S. H., Lee, S. H., Dang, D. T., Kwon, M. S., Chang, W. J., Yu, Y. J., ... Koo, Y. M. (2008). Enhanced stability of *Candida antarctica* lipase B in ionic liquids. *Korean Journal of Chemical Engineering, 25*(2), 291-294.

Hekmat, D., Hebel, D., Joswig, S., Schmidt, M., & Weuster-Botz, D. (2007). Advanced protein crystallization using water-soluble ionic liquids as crystallization additives. *Biotechnology Letters, 29*(11), 1703-1711.

Heller, W. T., O'Neill, H. M., Zhang, Q., & Baker, G. A. (2010). Characterization of the influence of the ionic liquid 1-butyl-3-methylimidazolium chloride on the structure and thermal stability of green fluorescent protein. *The Journal of Physical Chemistry B, 114*(43), 13866-13871.

Holbrey, J. D., & Seddon, K. R. (1999). The phase behaviour of 1-alkyl-3-methyl-imidazolium tetrafluoroborates; ionic liquids and ionic liquid crystals. *Journal of the Chemical Society, Dalton Transactions,* (13), 2133-2139.

Huang, J. L., Noss, M. E., Schmidt, K. M., Murray, L., & Bunagan, M. R. (2011). The effect of neat ionic liquid on the folding of short peptides. *Chemical Communications, 47*(28), 8007-8009.

Ikura, M., Kay, L. E., & Bax, A. (1990). A novel approach for sequential assignment of ^{1}H, ^{13}C, and ^{15}N spectra of larger proteins: Heteronuclear triple-resonance three-dimensional NMR spectroscopy. Application to calmodulin. *Biochemistry, 29*(4), 4659-4667.

Irimescu, R., & Kato, K. (2004). Lipase-catalyzed enantioselective reaction of amines with carboxylic acids under reduced pressure in non-solvent system and in ionic liquids. *Tetrahedron Letters, 45*(3), 523-525.

Johnson, B. A., & Blevins, R. A. (1994). NMR View: A computer program for the visualization and analysis of NMR data. *Journal of Biomolecular NMR, 4*(5), 603-614.

Judge, R. A., Takahashi, S., Longenecker, K. L., Fry, E. H., Abad-Zapatero, C., & Chiu, M. L. (2009). The effect of ionic liquids on protein crystallization and X-ray diffraction resolution. *Crystal Growth and Design, 9*(8), 3463-3469.

Kay, L. E., Ikura, M., Tschudin, R., & Bax A. (1990). Three-dimensional triple-resonance NMR spectroscopy of isotopically enriched proteins. *Journal of Magnetic Resonance, 89*(3), 496-514.

Kumar, A., Ernst, R. R., & Wüthrich, K. (1980). A two-dimensional nuclear Overhauser enhancement (2D NOE) experiment for the elucidation of complete proton-proton cross-relaxation networks in biological macro-molecules. *Biochemical and Biophysical Research Communications, 95*(1), 1-6.

Lange, C., Patil, G., & Rudolph R. (2005). Ionic liquids as refolding additives: N'-alkyl and N'-(ω-hydroxyalkyl) N-methylimidazolium chlorides. *Protein Science, 14*(10), 2693-2701.

Lau, R. M., Sorgedrager, M. J., Carrea, G., Van Rantwijk, F., Secundo, F., & Sheldon, R. A. (2004). Dissolution of *Candida antarctica* lipase B in ionic liquids: effects on structure and activity. *Green Chemistry, 6*(9), 483-487.

Lozano, P., De Diego, T., Carrié, D., Vaultier, M., & Iborra, J. L. (2001a). Over-stabilization of *Candida antarctica* lipase B by ionic liquids in ester synthesis. *Biotechnology Letters, 23*(18), 1529-1533.

Lozano, P., De Diego, T., Carrié, D., Vaultier, M., & Iborra, J. L. (2003). Enzymatic ester synthesis in ionic liquids. *Journal of Molecular Catalysis B: Enzymatic, 21*(1), 9-13.

Lozano, P., De Diego, T., Guegan, J. P., Vaultier, M., & Iborra, J. L. (2001b). Stabilization of α-chymotrypsin by ionic liquids in transesterification reactions. *Biotechnology and Bioengineering, 75*(5), 563-569.

Marszałł, M. P., & Kaliszan, R. (2007). Application of ionic liquids in liquid chromatography. *Critical Reviews in Analytical Chemistry, 37*(2), 127-140.

Muhandiram, D. R., & Kay, L. E. (1994) Gradient-enhanced triple-resonance three-dimensional NMR experiments with improved sensitivity. *Journal of Magnetic Resonance, Series B, 103*(3), 203-216.

Naushad, M., AL-Othman, Z. A., Khan, A. B., & Ali, M. (2012). Effect of ionic liquid on activity, stability, and structure of enzymes: A review. *International Journal of Biological Macromolecules, 51*(4), 555-560.

Noritomi, H., Minamisawa, K., Kamiya, R., & Kato, S. (2011). Thermal stability of proteins in the presence of aprotic ionic liquids. *Journal of Biomedical Science and Engineering, 4*(2), 94-99.

Oh, B. H., Westler, W. M., Darba, P., & Markley, J. L. (1988). Protein carbon-13 spin systems by a single two-dimensional nuclear magnetic resonance experiment. *Science, 240*(4854), 908-911.

Rodrigues, J. V., Prosinecki, V., Marrucho, I., Rebelo, L. P. N., & Gomes, C. M. (2011). Protein stability in an ionic liquid milieu: On the use of differential scanning fluorimetry. *Physical Chemistry Chemical Physics, 13*(30), 13614-13616.

Santoro, M. M., & Bolen, D. W. (1988) Unfolding free energy changes determined by the linear extrapolation method. 1. Unfolding of phenylmethanesulfonyl α-chymotrypsin using different denaturants. *Biochemistry, 27*(21), 8063-8068.

Sasmal, D. K., Mondal, T., Sen Mojumdar, S., Choudhury, A., Banerjee, R., Bhattacharyya, K. (2011). An FCS study of unfolding and refolding of CPM-labeled human serum albumin: Role of ionic liquid. *The Journal of Physical Chemistry B, 115*(44), 13075-13083.

Sen Mojumdar, S., Chowdhury, R., Chattoraj, S., & Bhattacharyya, K. (2012). Role of ionic liquid on the conformational dynamics in the native, molten globule, and unfolded states of cytochrome C: A fluorescence correlation spectroscopy study. *The Journal of Physical Chemistry B, 116*(40), 12189-12198.

Spera, S., & Bax, A. (1991). Empirical correlation between protein backbone conformation and Cα and Cβ ^{13}C nuclear magnetic resonance chemical shifts. *Journal of the American Chemical Society, 113*(14), 5490-5492.

Stefani, M., Taddei, N., & Ramponi, G. (1997). Insights into acylphosphatase structure and catalytic mechanism. *Cellular and Molecular Life Sciences, 53*(2), 141-151.

Stockman, B. J., Reily, M. D., Westler, W. M., Ulrich, E. L., & Markley, J. L. (1989). Concerted two-dimensional NMR approaches to hydrogen-1, carbon- 13, and nitrogen-15 resonance assignments in proteins. *Biochemistry, 28*(1), 230-236.

Summers, C. A., & Flowers, R. A. (2000). Protein renaturation by the liquid organic salt ethylammonium nitrate. *Protein Science, 9*(10), 2001-2008.

Van Rantwijk, F., & Sheldon R. A. (2007). Biocatalysis in ionic liquids. *Chemical Reviews, 107*(6), 2757-2785.

Weaver, K. D., Vrikkis, R. M., Van Vorst, M. P., Trullinger, J., Vijayaraghavan, R., Foureau, D. M., … Elliott, G. D. (2012). Structure and function of proteins in hydrated choline dihydrogen phosphate ionic liquid. *Physical Chemistry Chemical Physics, 14*(2), 790-801.

Wishart, D. S., Sykes, B. D., & Richards, F. M. (1991). Relationship between nuclear magnetic resonance chemical shift and protein secondary structure. *Journal of Molecular Biology, 222*(2), 311-333.

Wittekind, M., & Mueller, L. (1993). HNCACB, a high-sensitivity 3D NMR experiment to correlate amide-proton and nitrogen resonances with the alpha- and beta-carbon resonances in proteins. *Journal of Magnetic Resonance, Series B, 101*(2), 201-205.

Zhao, H., Campbell, S. M., Jackson, L., Song, Z., & Olubajo O. (2006a). Hofmeister series of ionic liquids: Kosmotropic effect of ionic liquids on the enzymatic hydrolysis of enantiomeric phenylalanine methyl ester. *Tetrahedron: Asymmetry, 17*(3), 377-383.

Zhao, H., Olubajo, O., Song, Z., Sims, A. L., Person, T. E., Lawal, R. A., & Holley, L. A. (2006b). Effect of kosmotropicity of ionic liquids on the enzyme stability in aqueous solutions. *Bioorganic Chemistry, 34*(1), 15-25.